International

WOCE

Newsletter

Number 23 July 1996

IN THIS ISSUE

Published by WOCE International Project Office at Southampton Oceanography Centre, UK

How Would You Answer Henry Stommel?

W. John Gould, Director, WOCE IPO, john.gould@soc.soton.ac.uk

I was recently asked – "If Henry Stommel were here today he might say – 'What have you learned about the ocean that you didn't know before WOCE started?'"

So how would we answer him? What have we learned that is new? I've tried to think about this and immediately came up with the following.

- Satellite altimetry has provided for the first time a global perspective on the circulation and its variability and enhanced the monitoring of sea level.
- Starting to understand the mismatch between oceanic flux estimates and those from models and air-sea fluxes.
- Measuring the magnitude and spatial extent of decadal-scale temperature and salinity changes.
- An estimate ($2 \times 10^{-5} m^2 s^{-1}$) of diapycnal mixing that is an unambiguous confirmation of previous estimates.
- WOCE has been a catalyst for new technology, notably the ALACE and PALACE floats that have given new insights into the zonal nature of mid-latitude currents. Better use of ADCP sensors.
- The output of eddy-permitting global models is now realistic enough to encourage detailed comparison with WOCE and other observations.
- WOCE tracer data have given us new insights into the pathways and rates of the thermohaline circulation.

This is a far from comprehensive list and I need your help to build up a set of answers so that we can demonstrate the success of WOCE. Most importantly we need to focus on results that are of relevance to climate research. Input to the IPO please.

These developments will be pieces of a WOCE jigsaw that will come together in the WOCE synthesis activity that is starting with the first regional workshop on the Pacific Ocean in Newport Beach, California 19–23 August. The first WOCE Newsletter of 1997 will report on that workshop and the lessons learned from it. In this Newsletter are announcements for the two 1997 regional workshops on the Southern Ocean and South Atlantic.

Meetings

There have been a number of meetings in recent weeks. The Synthesis and Modelling Working Group held its second meeting at the Southampton Oceanography Centre and is now preparing a strategy for the WOCE AIMS phase that will address both scientific and global funding and infrastructure issues. The SMWG also considered plans by WCRP for an Ocean Modelling Intercomparison Experiment (OMIP). The SMWG had some reservations about the overhead that such an intercomparison might impose but in general was supportive of the concept and will work with the CLIVAR Numerical Experimentation Group-2 to develop an OMIP strategy.

The final meeting of the WOCE/CLIVAR Surface Velocity Programme (SVP-8) was held in southern France. I must thank Peter Niiler and the members of the planning committee for their efforts through WOCE and TOGA to solve the problems of making reliable upper ocean current measurements and for finding resources to carry them out. After significant changes in objectives and management the SVP will now become a Global Drifter Program (GDP), operating under the WMO/IOC Data Buoy Co-operation Panel. The GDP will have a variety of interests ranging from CLIVAR to operational projects in GOOS to individual research programmes and to fully operational weather and climate prediction systems.

The CLIVAR SSG met in Japan and John Church (WOCE SSG Co-Chair) and I made presentations on the observations initiated by WOCE that would be of value if continued by CLIVAR and on the structure and function of the WOCE data system (see also article on page 38). While the CLIVAR SSG recognise the need to build on the experience of WOCE, it was also clear that a greater emphasis would be placed on the delivery of real-time data.

Finally I attended the first planning meeting for a WCRP Conference to be held in Geneva in August 1997. The purpose of the Conference – attendance will be primarily by invitation – will be to present to policy makers the achievements of WCRP in addressing climate issues of the type highlighted in the recent IPCC report. This Conference will be an important chance to emphasise the key role played by the oceans in the climate system.

Our own conference

Planning is intensifying for the WOCE Conference "Ocean Circulation and Climate" to be held in Halifax, Canada in 1998. Local and scientific organising committees have been formed (the latter chaired by Prof. Gerold Siedler) and a first announcement will be issued this autumn. A related issue is that of publications stemming from the Workshops and from the WOCE Conference. The SSG and SMWG are keen to have a coherent policy for making the results of WOCE readily accessible to a wide scientific readership. In light of this I will be exploring with publishers and with the workshop co-ordinators, the means by which this can be made possible.

This issue

This Newsletter contains a number of articles on WOCE tracer measurements and their interpretation. The impetus for this focus was the successful 1995 Maurice Ewing Symposium.

This is our second issue with a colour section. We hope you find this new innovation useful and that our almost 1000 recipients and many other readers benefit from keeping abreast of WOCE research.

Combining Passive Tracer Observations with Ocean Circulation Models

T.W.N. Haine, Atmospheric, Oceanic and Planetary Physics, University of Oxford, OX1 3PU, UK, twh@atm.ox.ac.uk

The WOCE community has invested heavily in observations of passive tracers to assist in estimating the planetary and decadal-scale ocean circulation and an unprecedented global database now exists. Oceanographers are beginning to interpret and synthesise these measurements in order to extract the information they contain about the large-scale flow. Observations of CFCs (chlorofluorocarbons) have been particularly abundant since these compounds are inert in sea-water with relatively well-known, time-varying, tropospheric histories. This article examines the general nature of the question "How do we combine tracer data with circulation models to constrain the flow?" using CFCs as a typical example.

Fig. 1 (page 19) shows CFC observations from two hydrographic sections in the Southern Ocean. The stations are shown in Fig. 2 with the anticipated path of Antarctic Bottom Water (AABW) from its source in the Weddell Sea along the foot of the south west Indian Ridge and into the abyssal Indian Ocean. The CFC data show a concentration maximum distinguishing this recently-ventilated boundary current from the interior deep and abyssal waters. This qualitative analysis is relatively unambiguous given that CFC concentrations have been steadily rising this century from a natural background of zero (Fig. 3). However, it is less clear how one might use the CFC distribution in a *qualitative* way.

To approach this question we write the equation governing the concentration field, C (a function of position $\mathbf{x} = (x, y, z)$ and time t), of a particular tracer species,

$$\frac{\partial C}{\partial t} + \mathbf{u} \cdot \nabla C = \nabla \cdot (K \nabla C) \qquad (1)$$

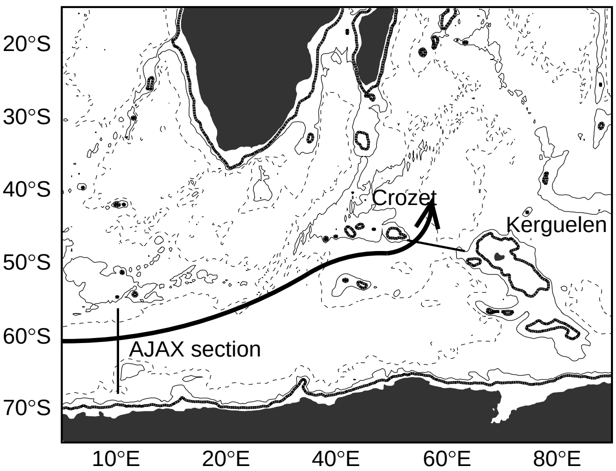

Figure 2. Topography of the Southern Ocean (1500 m, 3000 m and 4500 m isobaths shown). Section locations and the path of AABW are marked.

where $\mathbf{u}(\mathbf{x}, t)$ is the flow and K is a mixing coefficient relating the diffusive flux of C to the gradient of C. (Different processes may be represented by K (*e.g.*, molecular diffusion, eddy diffusion) depending on the scales of interest in the problem. K need not be constant). Equation (1) is accurate and succinct stating that the tracer is advected by the circulation and smoothed by mixing processes. There are no internal sources or sinks (for CFCs at least) and the tracer enters the surface ocean by exchange with the atmosphere. In a nutshell, the tracer interpretation question concerns the determination of $\mathbf{u}$ and K given measurements of C.

Interpretation of tracer data at a single point

A popular and pragmatic approach to solving (1) has been to write the interior concentration as a combination of two fundamental processes (*e.g.*, Pickart *et al*., 1989; Rhein, 1994). First, there is advection, with a time-lag due to transit from the ocean surface where the concentration is set. Second, there is a dilution due to the net effect of the irreversible mixing processes that K stands for. In other words, we write the concentration,

$$C(\mathbf{x}, t) = \frac{\mathrm{C}(\mathbf{x}_{surf}, t - \tau_{transit})}{\gamma} \qquad (2)$$

where the surface boundary concentration $\mathrm{C}(\mathbf{x}_{\mathrm{surf}}, t)$ (and its error) is well-known either by measurements or models of the air/sea interaction. $\tau_{transit}$ is the time for transit from $\mathbf{x}_{surf}$ to $\mathbf{x}$ and γ is a dimensionless quantity representing the dilution due to the mixing along this path. We assume that the location $\mathbf{x}_{surf}$ and the trajectory length, L, between $\mathbf{x}_{surf}$ and $\mathbf{x}$ are established so we can write the mean speed as, $u = L / \tau_{transit}$. Under certain conditions γ and $\tau_{transit}$ are functions of position only. These are:

(i) The flow is steady,

(ii) Mixing occurs with tracer-free water only.

This simple description supposes that the large-scale ocean circulation persists for many years in such a way that distinct water masses with specific characteristics and source regions are coherent over planetary distances. Clearly, there are objections to this view: the ocean shows variability at every scale. We shall avoid discussing these issues and, rather, use this simple approximation as an example of the general method of combining tracer data and circulation models.

The task is now to find γ and $\tau_{transit}$, and two robust limits can be immediately examined. First, assume there is no mixing whatsoever: the tracer is transported by advection alone: $\gamma = 1$, or $K = 0$. We have an upper limit on the transit time, or, equivalently, a lower limit on the average speed. For example, the data in Fig. 1 would give maximum speeds of 0.53 and 0.51 cm/s for the AJAX and ADOX sections respectively, taking the current core as the peak concentration in the abyssal CFC maximum. The second limit is for the case of $\tau_{transit} = \infty$, and the tracer transport is solely due to mixing processes. We have an upper limit on the dilution; 20 at AJAX and 19 at the ADOX line.

Although these limiting values are reliable (given our assumptions) they are not very informative because they lie outside reasonable oceanographic ranges. Clearly, both advection and mixing are important mechanisms for setting the interior tracer concentration.

To determine $\tau_{transit}$ and γ simultaneously one may use two tracer compounds with different time histories measured at the same place. The transit time is then equal to the ratio age, or ventilation age, used by many authors and defined by Haine and Richards (1995). Fig. 4 shows the results of such a calculation for the Southern Ocean CFC data. At the AJAX section (Fig. 1a) a range of possible combinations exists, rather than a unique pair. This is because only CFCs -11 and -12 were measured on this cruise and these compounds do not have independent source histories (legislation in the mid 1980s regulated their emissions). However, CCl_4 was measured in addition to CFCs 11 and 12 at the ADOX section and in this case a unique combination of $\tau_{transit}$ and γ exists; $\tau_{transit} = 29$ yrs corresponding to a mean speed of 1.0 cm/s, and $\gamma = 8$ at Crozet.

Combining data from different places

Given our assumptions we have found $\tau_{transit}$ and γ simultaneously using the CCl_4 data. But we have only used a fraction of the measurements available, and very few datasets include this compound. To make further progress we must combine the model with observations made at different places and times. This requires assumptions about how $\tau_{transit}$ and γ vary in space. Furthermore, the instrumental uncertainty may no longer be the appropriate data error as it was when we considered the interpretation of tracer data at a single point. There are now additional sources of error due to inadequate sampling of the tracer field, or temporal variability caused by eddies for example. These uncertainties are not well known but clearly play a crucial role as we shall see.

So, we must specify how $\tau_{transit}$ and γ depend on position. As a simple example assume that the transit time and dilution are given by,

$$\tau_{transit} = \frac{x}{u}, \gamma = 1 + \frac{kx}{uA_0} \tag{3}$$

where x measures the distance along the path of the boundary current from the Weddell Sea, u is a constant speed, k a constant transfer coefficient characteristic of the mixing process that causes the dilution and A_0 is the cross-sectional area of the plume at $x = 0$ (taken to be 10^{-7} m^2 here). Determining the values of u and k that give the best fit to the observations is an inverse problem and is straight-forward in this case. If we allow a data error of 20% we discover that (3) gives a good fit to the observations, otherwise we must reject the model as inconsistent with our measurements. Given the simplicity of the model this data error seems reasonable, although obviously we need to know in general the variability of the underlying tracer field. If we do accept the fit we find that $u = 1.10\,\mathrm{cm/s}$, $k = 0.12\,\mathrm{m^2/s}$ corresponding to transit times of 13 and 27 yrs and dilutions of 6 and 11 at the AJAX and ADOX sections respectively (Fig. 4).

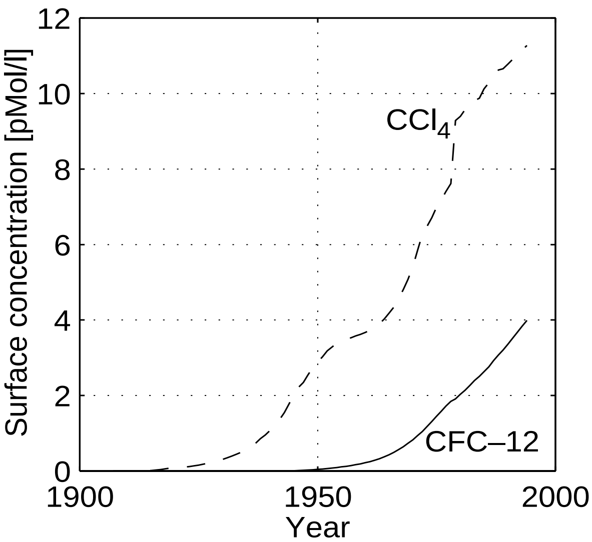

Figure 3. Concentration (pmol/l) history of CFC-12 and CCl_4 in surface waters of the Weddell Sea assuming 80% saturation with the atmosphere (as observed by A.J. Watson, pers. comm.).

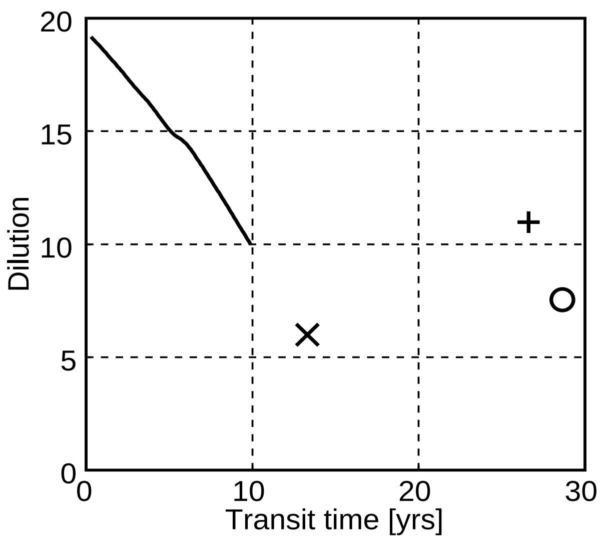

Figure 4. Solutions of $\tau_{transit}$ and γ from the simple transport models used in the text. Full line is fit to AJAX CFC-11 and CFC-12, o is ADOX CFC-11, CFC-12 and CCl_4, $\times$ and + are fits to both AJAX and ADOX data simultaneously ($\times$ shows values at AJAX section: + shows values at ADOX section).

A general method

Let us recap. In order to simplify the tracer interpretation problem a number of assumptions have been made. Given these, the tracer data constrain certain aspects of the circulation: in this case the average speed, or transit time, of a deep boundary current in the Southern Ocean and a measure of the mixing with surrounding waters. Although we have shown that the data are consistent with the model this does not imply that the model has been verified – clearly there are other possible assumptions we could have made. Before we accept the tracer-derived circulation parameters we must test how sensitive they are to a range of alternative possible assumptions. For example, other ways of allowing $\tau_{transit}$ and γ to vary (Eq. (3) may give radically different results.

Despite using a highly idealised model to represent Eq.(1) the method captures the essence of a general approach. Clearly, there is a vast amount of extra information, excluded from the simple model, that could be exploited to improve the analysis. For example, (3) could be replaced by dynamical laws connecting the current speeds to the density field – and hence to other observable quantities (temperature and salinity). Nevertheless, we would still need to make some restricting assumptions as we did in the simple example here. For instance, we may consider the circulation to be steady, and approximate the continuous equations using a finite resolution numerical model. As the amount of extra knowledge included in the synthesis increases, the inverse problem becomes much harder. However, its nature is the same: a statistical issue concerned with finding the best fit of model to data (*e.g.*, Memery and Wunsch, 1990; Wunsch, 1988). And finally, once we have found an answer (*i.e.*, an ocean circulation constrained by tracer data and other information), we will still have to test its sensitivity to alternative assumptions.

This task of combining passive tracer data with ocean circulation models to estimate the circulation is extremely demanding (both technically and computationally). Oceanographers are starting to meet this challenge as WOCE enters the analysis and modelling phase. The tantalising transient tracer fields of Fig. 1 have great potential but at this stage it is too early to say how they will improve knowledge of the large-scale mean circulation in a quantitative way.

References

Haine, T.W.N., and K.J. Richards, 1995: The influence of the seasonal mixed layer on the oceanic uptake of CFCs. J. Geophys. Res., 100, 10745–10754.

Memery, L., and C. Wunsch, 1990: Constraining the North Atlantic circulation with tritium data. J. Geophys. Res., 95, 5239–5256.

Pickart, R.S., N.G. Hogg and W.M. Smethie, 1989: Determining the strength of the Deep Western Boundary Current using the CFM ratio. J. Phys. Oceanogr., 14, 443–462.

Rhein, M., 1994: The deep western boundary current: Tracers and velocities. Deep-Sea Res., 12, 1154–1158.

Weiss R.F., J.L. Bullister, M.J. Warner, F.A. van Woy and P.K. Salemeh, 1990: AJAX expedition CFC measurements. SIO 90-6.

Wunsch, C., 1988: Eclectic modelling of the north Atlantic. II. Transient tracers and the ventilation of the eastern basin thermocline. Phil. Trans. Roy. Soc., 325A, 201–236.

Get Ready for the WOCE Pacific Workshop!

The WOCE Pacific Programme – Summary of Field Programme and Location of Data

The WOCE Data Information Unit (DIU) at Delaware has just published a summary of the WOCE Pacific Field Programme, ready in time for the first regional WOCE workshop to be held in Newport Beach, Califonia, 19–23 August this year.

The document attempts to identify all the components of the Pacific *in-situ* programme that have been carried out and to provide information on the current location of the basic data. It is arranged by observation type with most sections starting with a map showing the original planning for the observations. This is followed by a summary giving dates, PIs, and the DAC/DIU understanding of the status of the data.

To receive the document please contact the DIU:

e-mail: **woce.diu@diu.cms.udel.edu**
Fax: **+1-302-6454007**
Phone: **+1-302 6454240**

An electronic version is available on the WWW:

http://www.cms.udel.edu/~jimc

Tritium and ^{3}He in the WOCE Pacific Programme

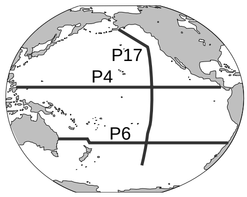

William J. Jenkins, Woods Hole Oceanographic Institution, Woods Hole, MA 02543, USA, wjenkins@whoi.edu

Introduction

The WOCE Pacific Survey has provided us with a large scale view of the distribution of tracers in the world's largest and perhaps the least sampled ocean basin. Of particular interest is the documentation of the passage of man-made tracers into the ocean, which provides us with information on the climatically important phenomenon of ocean ventilation. Ventilation occurs by the intertwined processes of water mass formation and transformation, circulation, mixing and destruction. These tracers also highlight subtler, but equally important processes of intergyre exchange and diapycnal mixing. The various tracers have differing time histories: some are more-or-less sharply spiked in time, while others increase monotonically with time. They also have differing patterns of deposition: some tracers were delivered to the ocean predominantly in the northern hemisphere, while others were more uniformly deposited. Sometimes these tracers behave differently within the water column. Because they have all been produced in greatest abundance in the latter half of this century, these tracers present oceanographers with similar patterns, highlighting entry points and pathways of recently ventilated water masses. But because they have differing "boundary conditions", these tracers offer unique information. I present here some of the tritium and ^{3}He results from the WOCE Pacific Survey, and describe some first order observations regarding their respective distributions. Some of the features described may be similar to features seen in other anthropogenic tracers (*e.g.*, CFCs), but some are quite unique to this tracer pair, largely because of their different time histories and behaviour in the environment. Tritium was produced largely by atmospheric nuclear weapons testing in the 1950s and 1960s, and delivered to the ocean by a combination of vapour exchange, river runoff and direct precipitation. The net character of this delivery is that the tritium was deposited in large part to the northern hemisphere in an impulse-like fashion centred around 1964. As the heaviest isotope of hydrogen, tritium travels almost solely as part of the water molecule.

Tritium is radioactive: it decays to ^{3}He with a half-life of 12.45 years. ^{3}He is a stable, inert isotope that does not partake in chemical or biological processes. We measure ^{3}He as an isotope ratio anomaly (there is a background of atmospheric helium dissolved in sea water), and correcting for a small isotope effect in solution and various atmospheric exchange processes, we can calculate the excess ^{3}He above natural background. Because ^{3}He may be regarded as "dead tritium", we will generally report the ^{3}He in the same units as we do tritium (TU) for comparison. Note that there is another source of non-atmospheric ^{3}He in ocean waters: primordial ^{3}He is released from volcanic and hydrothermal sources on the sea floor. We will begin by discussing this additional source, showing two zonal sections of deep helium (where the signal is strongest) and then demonstrating that the *tritiugenic* (tritium produced) component is dominant in the upper ocean. This will be followed by the presentation of a meridional section of tritium and ^{3}He, and an isopycnal map of tritium in the Pacific basin.

Finally, please note that space does not permit a more complete presentation of our results, and that this is a report of work in progress. The reader is invited to visit our world wide web site (http://kopernik.whoi.edu) and specifically our web page dedicated to our WOCE Pacific Survey results (http://kopernik.whoi.edu/wpac/wpac.html) to see more sections and maps.

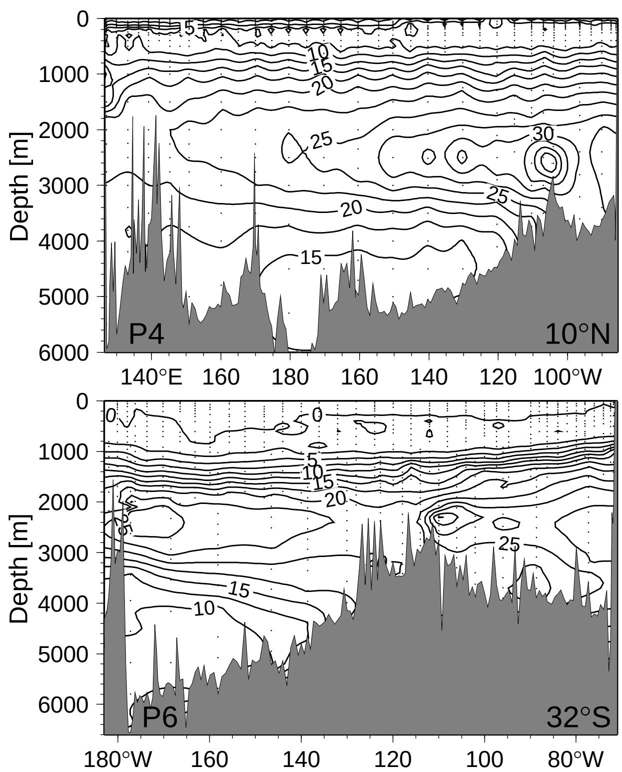

Figure 1. Two zonal sections of deep ^{3}He in the Pacific (east is on the right). The upper panel is along WOCE section P4 at 10°N, showing the large plume of primordial ^{3}He extending westward across the entire Pacific from the East Pacific Rise. The lower panel, along WOCE section P6 at 32°S, shows an eastward bound plume leaving the Rise, but also has the signature of two southward returning cores at the east and west ends.

Deep ^3He

The most striking feature of the global distribution of ^3He in the oceans has to be the large plumes of ^3He observed emanating from the East Pacific Rise. As a tracer of ocean circulation, primordial ^3He offers a unique characteristic of being injected into the water column at mid-depth, largely from a line source following the Rise crest. This provides oceanographers with an opportunity to trace Pacific Deep Water circulation in a way that no other tracer can. Fig. 1 shows two WOCE zonal sections of deep ^3He: P4 at 10°N and P6 at 32°S. The P4 section is dominated by strong ^3He maximum about 200 m above the East Pacific Rise crest, and the large tongue of ^3He extending westward from the East Pacific Rise (EPR) all the way across the basin. As the plume extends westward, it migrates upward across isopycnal surfaces: at the EPR the potential density anomaly referenced to 2500 db at the core of the ^3He maximum is close to $39.22\,kg/m^3$, but rises to less than 39.18 by the date line, and nearly $39.15\,kg/m^3$ by the eastern end of this section. Below this plume one sees relatively ^3He impoverished southern waters entering between the date line and the EPR crest.

The southern section shows a number of interesting features. In the west, one sees stronger signature of the invasion of low ^3He bottom waters from the south. At mid depths, there appear three cores of high ^3He. The first is an eastward-bound plume emanating from the Rise crest. Further, one can see indications of southward returning deep water at both the eastern and western ends of the section. These latter two features are distinguished from the EPR plume by their lighter density anomalies: the western one at $39.15\,kg/m^3$, and the eastern one at $39.19\,kg/m^3$, while the EPR plume is centred at $39.22\,kg/m^3$: the same as the plume at 10°N. The density anomaly of the western maximum suggests that it may be a signature of the returning deep water from the North Pacific. This suggestion is supported by the fact that there is an associated minimum in radiocarbon. The easternmost ^3He maximum is also associated with a radiocarbon minimum, suggesting a southward eastern boundary flow of deep waters at this latitude. Dr John Lupton (NOAA) has done much work with deep ^3He distributions, and has measured several other deep ^3He sections in the WOCE Pacific survey. He is currently compiling a more complete view of this unique tracer (see J. Lupton article, this issue, page 9).

Shallow tritium and ^3He

Fig. 2 shows a meridional section of tritium and ^3He *vs*. potential density anomaly for P17C along 135°W. The tritium section is characterized by a sharp front at the equator, with approximately four-to-five fold greater concentrations in the North. This is a result of the hemispherically asymmetric deposition of tritium in the early 1960s. Note also the tongue of tritium extending from the subtropics into the tropics. This feature was remarked upon by Fine and coworkers (Fine *et al*., 1987) and explained dynamically by McPhaden and Fine (1988).

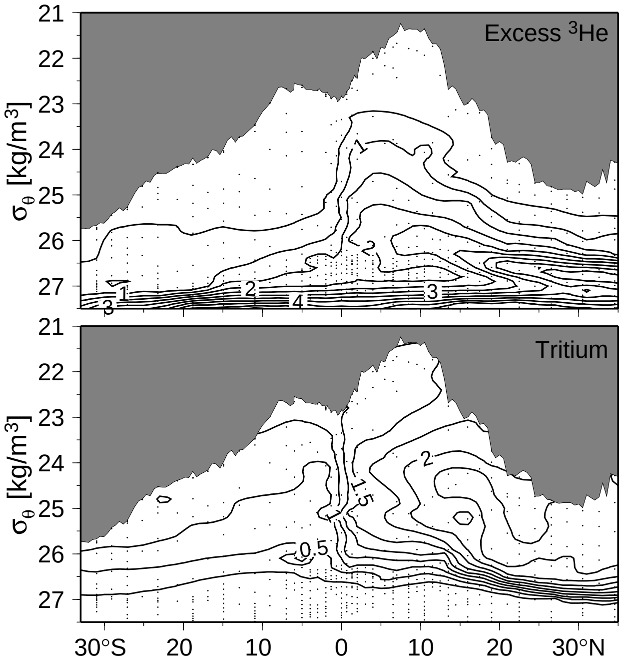

Figure 2. Tritium (lower panel) and Excess He (upper panel) in TU vs. potential density anomaly along WOCE section P17C at 135°W. Note the southward penetrating tongues of these tracers from the northern subtropics, sharp front in both properties at the equator, and the rising of the tracer isolines across density surfaces in the tropics.

The ^3He section shows a similar front at the equator, echoing the tritium distribution. However the most striking feature is the tongue of tritiugenic ^3He penetrating the tropics from the northern subtropics, and upwelling across isopycnals. This is a graphic signature of both intergyre exchange and upwelling.

The presence of the large, deep ^3He plumes raises some questions about distinguishing primordial from tritiugenic ^3He in the shallow waters. However, there are three reasons to suggest that there is little interference in the tritiugenic ^3He signal from the primordial signal below. First, several studies compute the primordial ^3He flux to be approximately $4-6\,atoms/cm^2/sec$. Noting that approximately 100 kg of tritium was deposited in the North Pacific from the bomb tests, one can compute a basin average production rate from the decay of this tritium to be approximately $40\,atoms/cm^2/sec$, or nearly ten times the primordial flux. As a side issue, one asks why the deep water plumes appear to be so impressive (the deep ^3He plume at 10°N is three or four times larger than the tritiugenic maximum)? The answer is that the deep waters are older and have accumulated the primordial flux for a much longer time. The second reason why the primordial influence may not be important in shallow waters concerns the circulation of the deep water. Recent calculations of water mass budgets in the Pacific indicate that the bulk of the Pacific Deep Water returns southward toward the Antarctic Circumpolar Current rather than upwelling through the main thermocline (Roemmich and McCallister, 1989; Wijffels *et al*., 1995). Thirdly, there is generally a ^{3}He minimum between the shallow tritiugenic ^{3}He maximum and the deeper primordial maximum. It is difficult to imagine significant vertical transport across this minimum.

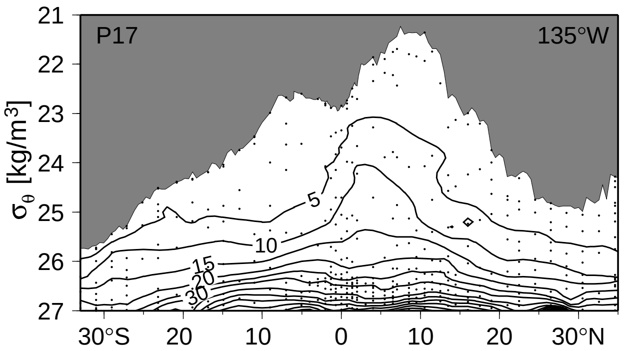

Figure 3. Tritium-^{3}He age (in years) vs potential density anomaly along WOCE section P17C at 135°W, computed from the sections shown in Fig. 2. Uncertainties in ages are a small fraction of a year near the surface, and increase with decreasing tritium concentration.

Thus we are emboldened to combine the tritium and excess ^{3}He data to compute the tritium-helium age, which is a measure of time elapsed since water was at the sea surface. This is shown for the P17C section in fig. 3. Some further caution should be exercised in the interpretation of the tritium-helium age, since it is affected in a non-linear fashion by mixing, especially for times greater than a decade or so. Thus our discussion at present is limited to some qualitative remarks.

The age contours ("isochrons") slope downward in isopycnal space away from the tropics, a result of equatorward flow at most depths. An age gradient along isopycnals is a measure of the meridional velocity component. For example, we see an age gradient between 20 and 30°N consistent with a meridional velocity of 1 cm/s for the $25.6\,kg/m^3$ isopycnal. This is consistent with geostrophic velocity estimates (*e.g*., Tsuchiya, 1982). Within the tropics, the isochrons rise up across isopycnals, marking the upwelling of waters which have entered from the subtropics. The tritium-helium age suggests an exchange time scale of order 10 to 15 years for this process, but a more complete analysis is required to gain further insight.

Fig. 4 (page 19) is a map showing the locations of stations sampled for tritium and ^{3}He by our laboratory, plotted on the distribution of tritium on the $26.8\,kg/m^3$ isopycnal surface. This isopycnal corresponds roughly to the North Pacific Intermediate Water salinity minimum in the North Pacific (Reid, 1973). The predominant features of the distribution of tritium on this surface are the pronounced north-south asymmetry and the strong minimum extending eastward from the South American coast. Note that the sharp decrease in tritium as one goes southward occurs north of 10°N, in contrast to the sharp equatorial front seen in the shallower layers (this can also be seen in Fig. 2). Also, there is a tongue of higher tritium extending eastward between the equator and about 8°N, suggesting zonal advection of this water mass from the west.

Missing from Fig. 4 are sections analyzed by Z. Top (RSMAS) along P14N and P16/17N in the North Pacific, and by P. Schlosser (LDEO) along S4 and several other sections in the Pacific sector of the Antarctic. Combined, we hope to have a more complete picture of the distributions of tritium and ^{3}He in the Pacific. As we acquire more of the WOCE Pacific Survey tracer data, we can build a more three dimensional view of the distributions of tritium, ^{3}He and tritium-helium age. The ultimate goal beyond these rough, qualitative descriptions, is the incorporation of these tracers into increasingly sophisticated circulation and exchange models. Within that context, they may be used to parameterize and perhaps even test or validate the models, allowing a better understanding of Pacific circulation and ventilation.

Work In progress

We are just now completing the helium and tritium analyses from all the samples taken in the WOCE Pacific Survey. The measurement process is a labour and time intensive activity which has been continuing from the very first WOCE Pacific line, and will be finished the end of this year. The reader is invited to visit our web page (mentioned earlier) to view our progress as we approach the finish line, and to share in our excitement as this most interesting story emerges and evolves.

We would like to end by expressing our gratitude to the many chief scientists who cooperated with us in obtaining our samples, and to the hard working marine technicians and ships' crew who made the acquisition of such a superb data set possible.

References

Fine, R.A., W.H. Peterson, and H.G. Ostlund, 1987: The penetration of tritium into the Tropical Pacific. J. Phys. Oceanogr., 17, 553–564.

McPhaden, M.J., and R.A. Fine, 1988: A dynamical interpretation of the tritium maximum in the central equatorial Pacific. J. Phys. Oceanogr., 18, 1454–1457.

Reid, J.L., 1973: The shallow salinity minimum of the Pacific Ocean. Deep-Sea Res., 20, 51–68.

Roemmich, D. and T. McCallister, 1989: Large scale circulation of the North Pacific. Prog. Oceanogr., 22, 171–204.

Tsuchiya, M. 1982: On the Pacific upper-water circulation. J. Mar. Res. 40S, 777–799.

Wijffels, S.E., J.M. Toole, H.L. Bryden, R.A. Fine, W.J. Jenkins and J.L. Bullister, 1995: The water masses and circulation at 10°N in the Pacific. Deep-Sea Res. (in press).

WOCE ^{3}He Measurements Enhance Our Understanding of the Deep Pacific Circulation

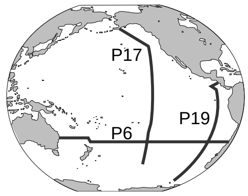

John Lupton, NOAA Pacific Marine Environmental Laboratory, Newport, OR 97365, USA, lupton@new.pmel.noaa.gov

Measurements of ^{3}He along WOCE Hydrographic Programme (WHP) sections have added greatly to our knowledge of the location and extent of hydrothermal plumes in the deep Pacific, thereby providing constraints on the deep circulation patterns. Helium is a useful tracer for deep ocean circulation because it is stable and conservative, and because the helium in the volcanic rocks derived from the Earth's mantle is tenfold enriched in ^{3}He/^{4}He relative to atmospheric helium. Thus the volcanic activity and associated hydrothermal circulation along the global mid-ocean ridge system introduces a ^{3}He-rich helium signal into the deep ocean basins which can be used to trace patterns of ocean circulation and mixing. This is especially true for the Pacific Ocean, where the spreading rate of the ridges is the greatest, resulting in a correspondingly high rate of mantle helium injection.

The WOCE Pacific lines P17 and P19 provide long meridional sections through the region of the huge helium plume emanating from the crest of the East Pacific Rise (EPR) at ~14°S (Fig. 1). This plume, which was first reported by Lupton and Craig (1981), exhibits a striking asymmetry suggesting westward transport in this region of the deep Pacific, in direct disagreement with the eastward flow described in the geostrophic circulation model of Stommel and Arons (1960). As might be expected, the existence of this deep ^{3}He plume spawned several additional theoretical and field studies. In a careful analysis of existing hydrographic data, Reid (1982) showed that a faint thermal plume with ~0.020°C excess temperature is present on the same isopycnal as the helium plume. In a very provocative paper, Stommel (1982) suggested that the helium plume may be an active feature in which the heat flux associated with hydrothermal input drives a pair of circulation cells which extend westward from a north-south trending ridge such as the EPR. Subsequent papers by Speer (1989) and Hautala and Riser (1993) directly addressed this question of whether hydrothermal input is driving the deep circulation in this region.

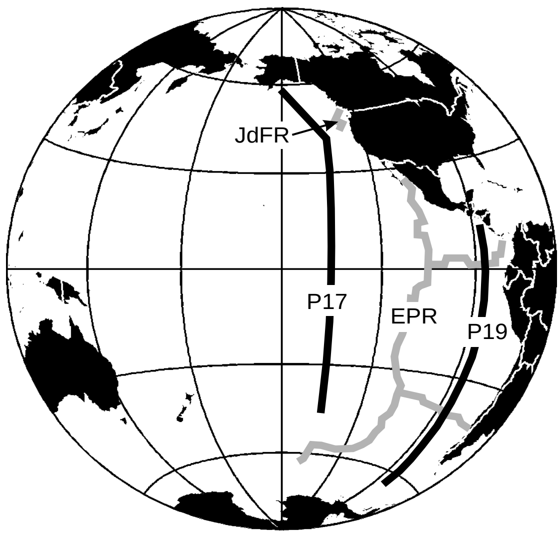

Figure 1. Map showing location of WHP lines P17 and P19 relative to the East Pacific Rise (EPR) and the Juan de Fuca Ridge (JdFR).

The deep ^{3}He measurements along P17 and P19 are shown in Fig. 2 (page 21). P17, along 135°W about 2500 km west of the EPR axis, shows three distinct deep maxima in δ^3He, each corresponding to a section through a distinct hydrothermal plume. The strongest maximum at 12–13°S and 2500 m depth is the southern EPR helium plume reported by Lupton and Craig (1981), while the slightly weaker maximum centred at ~8°N is another westward trending plume generated by hydrothermal input on the EPR at 8–12°N. The third maximum at ~42°N and (JdFR) 2000 m depth is helium from the Juan de Fuca Ridge in the far northeast Pacific. The shallower depth of this plume is a direct consequence of the shallower average depth of the Juan de Fuca Ridge axis compared to the EPR. The nearly symmetric pattern of two helium maxima at 12°S and 8°N with a minimum on the equator is a very striking feature of the deep helium field which is not easily matched in tracer models. While the symmetric helium maxima imply westward transport of tracer at these latitudes, the minimum on the equator suggests the presence of a deep eastward equatorial jet. Although this double plume structure was evident in the Geosecs eastern Pacific ^{3}He section, only recently have papers by Craig (1990) and Talley and Johnson (1994) drawn attention to the significance of this feature. While P17 sampled the deep Pacific directly west of the EPR crest, P19 along 88°W occupies an almost symmetric location about 2200 km to the east of the EPR axis. In agreement with the previous descriptions of westward trending plumes, the P19 deep helium section shows much weaker signals overall compared to P17. In particular, the strong maximum at 12°S in P17 is completely absent at P19, while another weaker maximum in δ^3He appears in P19 at ~28°S directly over the Nazca Ridge. The northern end of P19 has higher ^{3}He values where the line crosses the actively spreading Galapagos Rift. At the far northern end of the section, the Guatemalan Basin appears to be moderately enriched in ^{3}He, presumably due to hydrothermal input from the EPR and the Galapagos Rift.

Our knowledge of the south Pacific helium plume is summarized in Fig. 3, which shows δ^3He contoured in plan view on a surface at 2500 m depth, which is the depth of the ^{3}He maximum (Lupton, 1995). The figure includes deep helium data from Helios expedition, RITS-89, and from WHP lines P17, P19, and P6. While the main features of the jet-like helium plume were mapped during Helios Expedition (Hautala and Riser, 1993) and during NOAA's RITS-89 expedition along 105°W, the sampling on these earlier expeditions was confined mainly to the region between 5°S and 25°S. As shown in the figure, the WHP lines in his region have extended our coverage of the deep helium field, revealing a complex plume structure. In particular, P6 and P19 confirm the existence of a secondary plume extending eastward from the EPR axis at ~30°S. This is shown very clearly in the deep helium section along P6 reported by Jenkins (1996a), which shows a deep maximum in ^{3}He centred over the EPR axis and extending eastward into the Chile Basin. The map also reveals two regions where the gradient in δ^3He is remarkably high: one to the east of the EPR crest between 8°S and 20°S, and another to the west of the EPR axis at ~25°S latitude.

It is of interest to compare the deep ^{3}He field with other descriptions of the deep circulation in this region. For comparison, Fig. 3 includes the steric height calculations of Reid (1981) for 2000 db relative to 3500 db (dashed lines). While this estimate of the deep flow admittedly rests on several assumptions, it agrees remarkably well with the deep helium field. Considering that the local helium source is the EPR axis, the gyre in the upper left portion of the figure is consistent with the helium jet extending westward from the EPR, and Reid's broad eastward flow at 25–30°S coincides almost perfectly with the secondary helium plume centred at 30°S. Reid (1986) had previously generated a map very similar to Fig. 3 by comparing his steric height anomaly to the pattern of hydrothermal Mn and Fe recorded in the sediments. The fact that helium in the water column and hydrothermal Mn and Fe in the sediments are distributed in almost identical patterns implies that both the hydrothermal activity and the deep circulation in this region have been stable for thousands of years.

WHP deep helium measurements have also helped to map hydrothermal plumes in the vicinity of the Hawaiian Islands. It has been known for several years that Loihi Seamount, an active volcano on the southeastern flank of the Island of Hawaii, has hydrothermal vents near its summit (~1000 m depth) which produce detectable water-column hydrothermal plumes. In 1991 and 1994, helium profiles collected in the vicinity of Hawaii showed distinct maxima in δ^3He at 1100 m depth. Although the stations nearest to Hawaii exhibited the strongest signals (up to δ^3He = 28%), this distinct plume layer was detectable up to 400 km north of the Hawaiian Islands. A detailed comparison of the isotopic signature in this 1100-m deep plume layer versus deeper mid-ocean ridge plumes showed that this shallower plume has its origin on Loihi Seamount (Lupton, 1996).

In order to map the basin-scale extent of this Loihi plume, it was necessary to draw from several expeditions spanning the central Pacific region. Fig. 4 is a summary map of δ^3He at 1100 m depth, combining data from 8 different expeditions, including 5 WHP sections. The figure shows an extensive ^{3}He plume emanating from Hawaii and extending some 5000 km to the east. In contrast to its broad longitudinal extent, the Loihi plume seems to be confined to the latitude range from 12°N to 28°N. For example, the Loihi signal does not appear to penetrate as far south as the WHP P4 section along 9°N (Jenkins, 1996b). P17 crosses the Loihi plume in its mid-section, and yet the Loihi plume does not appear as a distinct plume core on P17 (Fig. 2). However, careful inspection of the P17 deep helium section reveals that the Loihi plume is expressed as an upturning of the δ^3He contours between 900–1200 m depth between latitudes 15°N and 25°N.

The asymmetry of the Loihi helium plume implies eastward transport at this depth in central north Pacific (Lupton, 1996). This flow is in conflict with most other descriptions of the Pacific circulation at ~1000 m depth, including those of Reid and Mantyla (1978) and Talley (private comm.). Furthermore, P4 along 8.5°N shows clear evidence of westward transport of ^{3}He from the EPR at 2500 m depth, thereby implying considerable shear in this region of the Pacific. Additional sampling in the vicinity of the Hawaiian Islands should enhance our picture of this Loihi plume, especially in the near field.

In this short note I have discussed one example where a well-defined ^{3}He signal provides strong constraints on the deep Pacific

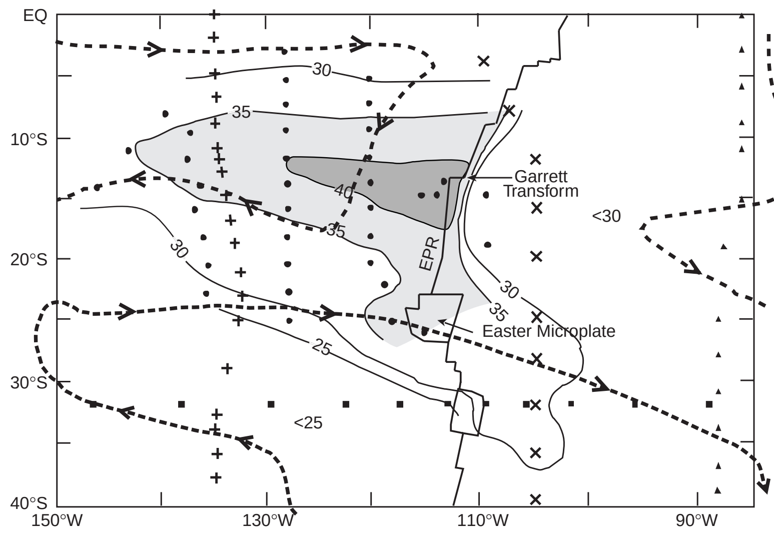

Figure 3. Map of δ^3He% contoured on a surface at 2500 m depth for a part of the south eastern Pacific. Contour interval is 5% in δ^3He. The bold lines mark the location of the spreading axis of the East Pacific Rise. The dashed lines indicate the steric height flow patterns at 2000 db relative to 3500 db from Reid (1981). Helium data are from Helios Expedition (filled circles), NOAA RITS-89 (crosses), WHP P17 (plusses), WHP P19 (filled triangles), and WHP P6 (filled squares). All helium measurements made at NOAA/PMEL except WHP P6, which were reported by Jenkins (1996a).

circulation. In this region WOCE deep helium measurements have greatly aided the process of defining the deep helium field. However, the big picture is much more important. When all of the WHP helium measurements are completed, we will have a fairly comprehensive map of both helium and tritium in the world ocean. This will provide a detailed tracer field which can be used in inverse model studies and also compared against forward tracer models.

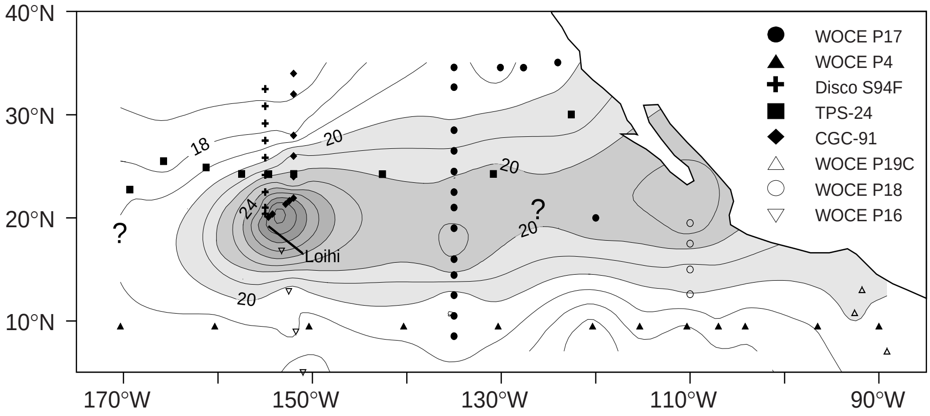

Figure 4. Map of δ^3He% contoured on a surface at 1100-m depth showing the broad lateral extent of the Loihi plume. Contour interval is 1% in δ^3He. The figure includes data from 8 different expeditions. Helium data along WHP lines P4 and P16 were provided by Jenkins (1996b, and private comm.). Figure taken from Lupton (1996).

References

Craig, H., 1990: The Helios helium-3 section: implications for the deep water circulation in the North and South Pacific. EOS Trans. AGU 71, 882.

Hautala, S.L., and S.C. Riser, 1993: Anonconservative–spiral determin-ation of the deep circulation in the eastern south Pacific. J. Phys. Ocean. 23, 1975–2000.

Jenkins, W.J., 1996a+b. Data for the WHOI Helium Isotope Group reported for WHP line P6+P4 at the following web site: http://kopernik.whoi.edu/wpac/p6dh.gif.

Lupton, J.E., 1995: Hydrothermal plumes: near and far field, in Seafloor Hydrothermal Systems: Physical, Chemical, Biological, and Geological Interactions, edited by S. Humphris *et al*. Geophysical Monograph 91, American Geophysical Union, Washington, D.C., pp. 317–346.

Lupton, J.E., 1996: A far-field hydrothermal plume from Loihi Seamount. Science 272, 976–979.

Lupton, J.E., and Craig, H., 1981: A major ^{3}He source on the East Pacific Rise, Science 214, 13-18, 1981. Reid, J.L., On the mid-depth circulation of the world ocean. In Evolution of Physical Oceanography, B.A. Warren and C. Wunsch, Eds., pp. 70–111, MIT Press, Cambridge, Mass.

Reid, J.L., 1982: Evidence of an effect of heat flux from the East Pacific Rise upon the characteristics of mid-depth waters. Geophys. Res. Lett. 9, 381.

Reid, J.L., 1986: On the total geostrophic circulation of the south Pacific Ocean: flow patterns, tracers and transports. Progr. Oceanogr., 16, No. 1, 1–61.

Reid, J.L., and A.W. Mantyla, 1978: On the mid-depth circulation of the North Pacific Ocean. J. Phys. Ocean. 8, 946–951.

Speer, K.G., 1989: The Stommel and Arons model and geothermal heating in the South Pacific, Earth Planet. Sci. Lett. 95, 359–366.

Stommel, H., 1982: Is the South Pacific helium-3 plume dynamically active? Earth Planet. Sci. Lett. 61, 63–67.

Stommel, H., and A.B. Arons, 1960: On the abyssal circulation of the world ocean. Part II – An idealized model of circulation pattern and amplitude in oceanic basins. Deep-Sea Res. 6, 217–233.

Talley, L., and G.C. Johnson, 1994: Deep, zonal subequatorial currents. Science 263, 1125–1128.

The Deep Western Boundary Current in the Tropical Atlantic: Deep Water Distribution and Circulation off Brazil

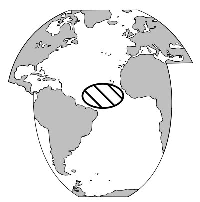

M. Rhein, F. Schott, L. Stramma, J. Fischer, O. Plähn and U. Send, Institut für Meereskunde an der Universität Kiel, Düsternbrooker Weg 20, 24105 Kiel, Germany, mrhein@ifm.uni-kiel.de

The importance of the Deep Western Boundary Current (DWBC) in the Atlantic for the interhemispheric exchange of water masses and of heat is well known, but data to estimate transports and to follow its pathways are sparse. New insight into the distribution of deep water masses, their circulation, transports and variability in the tropical Atlantic off Brazil was gained on four WOCE cruises (RV Meteor cruises in October 1990, May–June 1991, November 1992 and February–March 1994). Tracer and hydrographic data were taken along meridional sections at 44°W and 35°W and along zonal sections at 5°S and 10°S. In 1994, additional measurements were carried out along 40°W and along 4°30'N and the 44°W section was extended to the Mid Atlantic Ridge (Fig. 1). Direct velocity profiles were obtained by lowered ADCP and a Pegasus profiling system. The analysis of the data set is still in progress. In the following we summarize our results for the deep waters, obtained from from the combination of hydrography, tracers, geostrophy and direct velocity measurements, which were already published, are in press or submitted (Rhein, 1994; Rhein *et al*., 1995; Fischer *et al*., 1996; Rhein *et al*., 1996a,b,c; Rhein, 1996).

A relatively new tool in oceanography is the analysis of transient tracer measurements, like the Chloro-

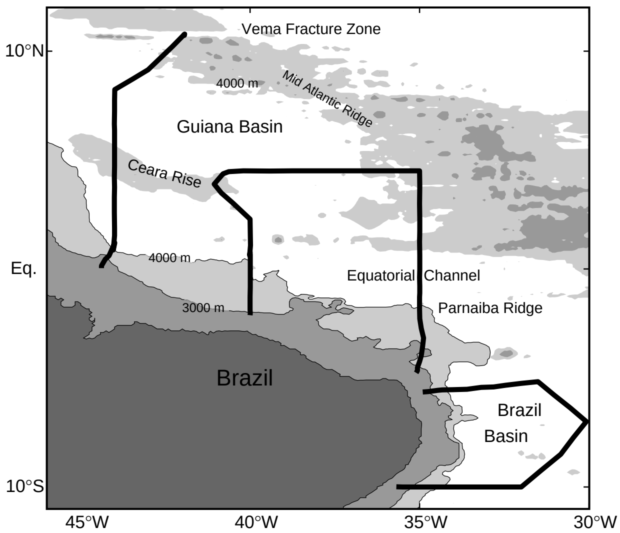

Figure 1. Sections, RV Meteor cruise M27/3, February–March 1994

fluorocarbons (CFCs, components CFC-11 and CFC-12). During the past several decades, the atmosphere and the upper ocean have been tagged with CFCs that had previously not existed in the environment. The CFCs are introduced into the deep ocean in regions of deep water formation like the northern North Atlantic. The newly-formed deep water masses proceed south in the DWBC, taking with them their unique CFC signal. Flowing along the continental margin of the American continent, the southward flowing DWBC between about 1200 and 4000 m encounters water of southern origin, with a northward flow of Antarctic Intermediate Water above and of Antarctic Bottom Water (AABW) below.

In the tropical Atlantic, two depth layers with CFC maxima are observed in the DWBC (Fig. 2a-d on page 20). The deep CFC maximum around 3800 m (Overflow Lower NADW: OLNADW) consists of water, which was formed by deep wintertime convection north of Iceland before overflowing the Denmark Strait and descending to greater depths. The upper maximum is found in 1600–1800 m depth and characterizes the shallowest part of the North Atlantic Deep Water (SUNADW), which could only be identified as a distinct water mass by its CFC and tritium signals. It is presumably formed in the southern Labrador Sea. Probably due to the weakening of the deep convection in the Labrador Sea in the mid 1970s and early 1980s, there is no distinct CFC signal in the Labrador Sea Water (LSW) in the tropical Atlantic. This also holds for the overflow water entering the Atlantic through the gaps between Iceland and Scotland (LNADW - old). The CFC signal of both, the OLNADW and the SUNADW decrease while flowing east and south in the tropical Atlantic.

The atmospheric CFC increase with time should be reflected by an accompanying increase in the CFC concentrations of SUNADW and OLNADW in the tropical Atlantic in the period 1990 to 1994 and the annual percent change should decrease. Both features, the CFC increase and the annual percent change decrease, are likely to be weakened in amplitude by mixing with older water and with surrounding water masses on the way from the formation region to the tropical Atlantic. In general, the mean CFC concentrations in the SUNADW and OLNADW off Brazil increase with time along the individual sections. However, the temporal increase was not continuous, and there was even a decrease at 5°S between 1992 and 1994. The annual percent change in the mean CFC-11 concentration of SUNADW varied between +23% per year and -14% per year with no spatial or temporal trend. The locally different linear correlations of the CFC maxima with salinity maxima in the SUNADW suggest that variability in the mixing history and in the spreading paths of the SUNADW have a significant impact on the tracer field in the tropical Atlantic. The arrival of more saline and thus less diluted SUNADW increased the observed CFC concentrations.

The cruise data and the mooring data at 44°W (Schott *et al*., 1993) revealed, that the variability in the deep flow field off Brazil is high, but some features seem to be persistent and, especially in the OLNADW, seem to be correlated with the tracer extrema. At 44°W, the upper CFC maximum of the SUNADW extends north (Fig. 2a), presumably caused by the recirculation of this water mass in the tropical Atlantic (Richardson and Schmitz, 1993). The OLNADW core at 3800 m depth is split by the Ceara Rise at 5°N. This pattern is consistent with the flow field characterized by eastward flowing cores south of Ceara Rise and at the northern flank of the rise (Fig. 3b).

At 35°W the water masses with high CFC values (Fig. 2b) exhibit the highest velocity signals. The flow cores of the individual water masses do not extend vertically over several layers but are found at different horizontal locations. In contrast to the DWBC at 44°W, the main transport of SUNADW and LSW is not trapped to the coast, but occurs about 320 km offshore (Fig. 3b). The flow pattern of the high tracer OLNADW is guided by the Parnaiba Ridge (1°45’S, 35°W), where the highest velocities and also the highest CFC concentrations were measured (Fig. 2b, 3c). In addition, a sporadic transport of OLNADW at the northern edge of the Equatorial Channel occurs.

The differences of the CFC signals (Figs. 2b, c) and the θ-S characteristic between the 35°W and the 5°S section suggest that a major modification of this water mass occurs between the two sections. The velocity fields of the various NADW water masses at 5°S are more vertically coherent than at 35°W, and the highest velocity signals are not restricted to the water masses with a high CFC concentrations. The main southward flow at 5°S occurs near the coast and is limited offshore by a reverse flow. At 10°S, the CFC signal of the OLNADW is smaller than the CFC concentrations of the northward flowing AABW near the bottom (Fig. 2d). The CFC-11 increase from 10°S to 11°N, mainly in the upper part of the tracer-poor AABW, reveals the mixing of AABW along its path with the above located CFC rich OLNADW. While propagating north, the AABW shifts to higher salinities at a given temperature.

The extended data set of the Meteor cruise in spring

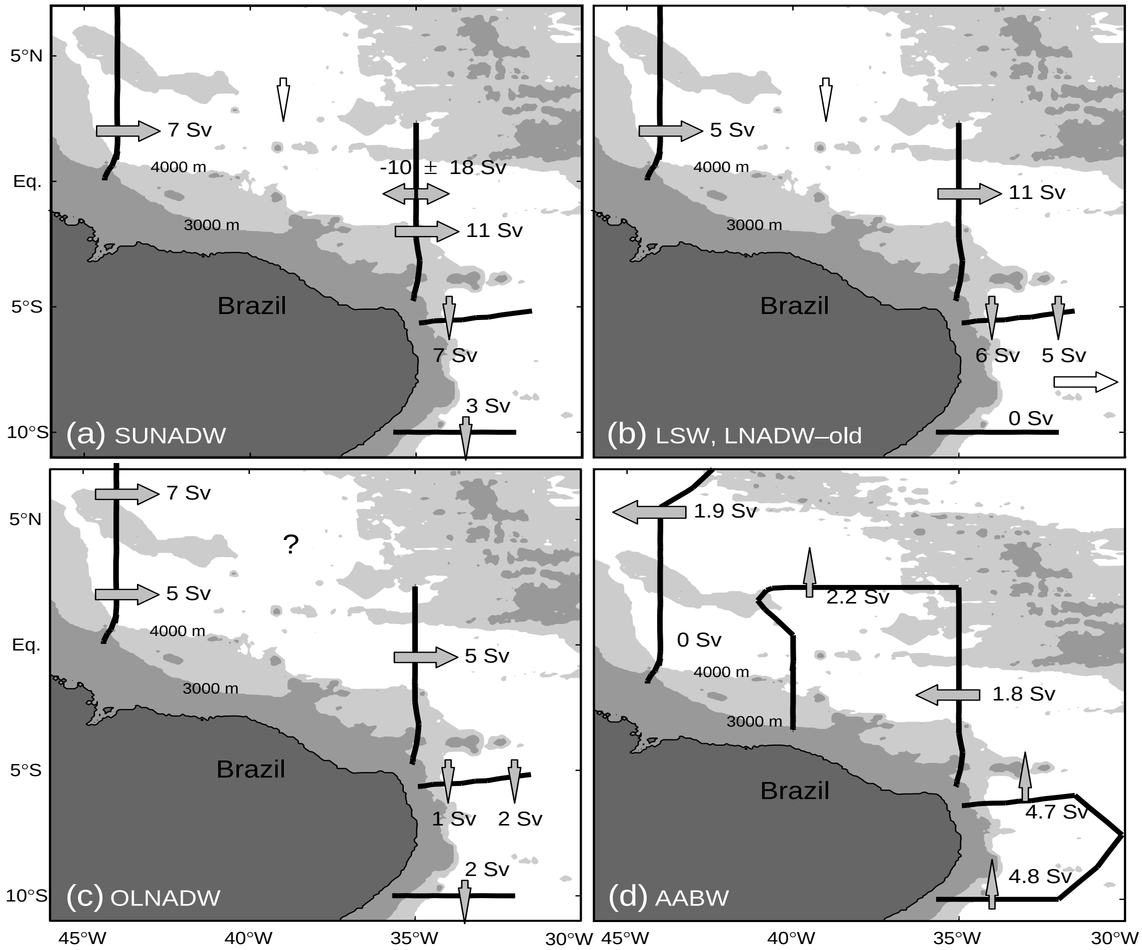

Figure 3. Circulation pattern for (a) SUNADW, (b) LSW and LNADW-old, (c) OLNADW and (d) AABW. The transport estimates are obtained from a combination of our results and previously published data. Open arrows are deduced from mass balance considerations.

1994 was used to study the circulation and transport of the AABW from 10°S to 11°N (Fig. 3d). The westward transport of AABW through the Equatorial Channel at 35°W was estimated to 1.5–1.8 Sv, which is about one third of the northward flowing AABW at 10°S and at 5°S west of about 31°30' W. The remaining flow recirculates, partly flowing through the Romanche Fracture Zone near the equator into the eastern Atlantic. West of 40°W, the sloping topography and the strong, eastward flowing DWBC presumably prevent the AABW from flowing west, thus it has to turn north at the eastern slope of the Ceara Rise. At 44°W, AABW flows west in the interior of the basin north of Ceara Rise in a main core near 7°15’N with a small return flow north of 8°43’N. A large fraction of the AABW enters the eastern Atlantic through the Vema Fracture Zone (VFZ) near 11°N, leaving only 0.3 Sv of AABW for the western Atlantic basins. The comparison of the water mass properties (T, S, CFCs) in the VFZ with stations in the Guiana Basin, the Equatorial Channel and in the Brazil Basin suggest a significant contribution of the NADW to the entire bottom water layer in the VFZ. The bottom water transport was obtained by a combination of geostrophic calculation and direct current observations with LADCP.

Summary

The cruise data and the mooring data at 44°W (Schott et *al*., 1993) showed the importance of the temporal variability for the deep velocity field off Brazil. Therefore the estimated flow fields of the deep water masses (Fig. 3) are not likely to reflect the long term mean transport, and one has to be cautious in the interpretation of these estimates. However, some of the observed flow features seemed to be persistent. The calculated transports for the deep water masses, 26.8±7.0 Sv at 35°W and 19.5±5.3 Sv at 5°S, are in the range of previously published estimates, but show the important influence of temporal and spatial variability.

The CFC distributions and the hydrographic measurements enabled us to identify four different components of NADW. Two of them, the SUNADW (around 1600 m depth) and the OLNADW (around 3800m depth) are characterized by a distinct CFC signal. For the OLNADW, the CFC distribution in general correlates with the flow field. For the SUNADW, the tracer and salinity fields as well as the observed velocity field reflect the various recirculation paths of this water mass. The temporal evolution of the CFC signals off Brazil from 1990–1994 indicate, that variability in spreading and mixing of the tracer bearing deep water masses might obscure the expected CFC increase with time. Thus for regions, remote from the formation areas of the deep water masses, great care has to be taken in the interpretation of the temporal evolution of the tracer signal.

References

Fischer, J., M. Rhein, F. Schott und L.Stramma, 1996: Water masses and transports in the Vema Fracture Zone. Deep-Sea Res., in press.

Rhein, M., 1994: The Deep Western Boundary Current: tracers and velocities. Deep-Sea Res. 41, 263–281.

Rhein, M., 1996: Estimating the mean transport of the Atlantic Deep Western Boundary Current using tracers. in AGU Monograph on the application of trace substances in Oceanography, P. Schlosser and W.M. Smethie, eds., submitted.

Rhein, M., L. Stramma and U. Send, 1995. The Atlantic Deep Western Boundary Current: Water masses and transports near the equator. J. Geophys.Res., 100, 2441–2457.

Rhein, M., L. Stramma and G. Krahmann, 1996a: The spreading of Antarctic Bottom Water in the Tropical Atlantic. J. Geophys Res., submitted.

Rhein, M., F. Schott, J. Fischer, U. Send and L. Stramma, 1996b: The Deep Water Regime in the Equatorial Atlantic. In: The South Atlantic: Present and Past Circulation, eds., G. Wefer, H. Berger, G.Siedler and D.Webb, Springer Verlag, in press.

Rhein, M., O. Plähn, R. Bayer, L. Stramma, and M. Arnold, 1996c: The temporal evolution of the tracer signal in the Deep Western Boundary Current, tropical Atlantic. In AGU Monograph on the application of trace substances in Oceanography, P. Schlosser and W.M. Smethie, eds. submitted

Richardson, P.L., and W.J. Schmitz, Jr., 1993: Deep cross-equatorial flow in the Atlantic measured with SOFAR floats. J. Geophys. Res., 98C, 8371–8387.

Schott, F., J. Fischer, J. Reppin and U. Send, 1993: On mean and seasonal currents and transports at the western boundary of the equatorial Atlantic. J. Geophys. Res., 98C, 14353–14368.

On Tracer Derived Ages in the Atlantic Isopycnic Model

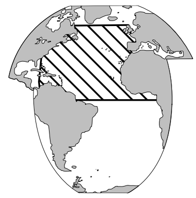

Yanli Jia, Southampton Oceanography Centre, Empress Dock, Southampton, SO14 3ZH, UK, yanli.jai@soc.soton.ac.uk

Transient tracers such as tritium, helium and CFCs (CFC-11, CFC-12, and CFC-113) have been used in many different contexts in the study of the ocean circulation. Observationalists use them to trace circulation pathways and estimate ventilation rates and the transport in the ocean (*e.g.*, Fine and Molinari, 1988; Doney and Jenkins, 1994). Modellers make use of the observations to validate ocean models (England *et al.*, 1994; Jia and Richards, 1996). Much effort has been made in collecting tracer data during the WOCE, and improved numerical models are now suitable for tracer simulations.

The Atlantic Isopycnic Model (AIM) is an isopycnic coordinate ocean general circulation model comprising a Kraus-Turner mixed layer and 19 constant potential density layers in the vertical. It has a horizontal resolution of 1° x 1°. It is an implementation of the Miami isopycnic coordinate ocean model (*e.g.*, Bleck *et al.*, 1992). A detailed description of AIM is given by New *et al.* (1995), and an analysis of a simulation of tritium and helium with this model is presented by Jia and Richards (1996). A simulation of CFC-11, CFC-12 and CFC-113 with the same model is reported here.

The combination of a set of tracers (*e.g.* tritium/helium pair, CFC-11/CFC-12 pair) can be used as a dating tool to provide estimates of the age of water. However, the ages derived from these tracers are subject to error mainly due to the oceanic mixing processes and the surface boundary conditions used. In the ideal case, we assume that the age of water in the ocean surface (or the mixed layer) is zero, and the age increases as soon as the water is subducted into the oceanic interior. In the case of the tritium/helium pair, the decay property of tritium to helium is used. If the concentration of helium in the surface water is assumed to be zero (then the tritium-helium age in the surface water or the mixed layer is zero), the age of water in the interior of the ocean will only be affected by mixing processes associated with the gradients of the tracers (Thiele and Sarmiento, 1990). For CFCs (either the CFC-11/CFC-12 pair, or the CFC-11/CFC-113 pair), the age is estimated using the ratio of their atmospheric concentrations. In this case, only when the saturation levels of the pair are the same, do we get zero age in the mixed layer (Haine and Richards, 1995). Otherwise, positive or negative age can occur in the mixed layer, which, when the water is subducted, will result in additional error in the estimated age of water in the oceanic interior.

In the next section, we will examine the processes which affect the estimate of the age of water by comparing the ideal age (for ideal age definition, see Thiele and Sarmiento, 1990), the tritium-helium age and the CFC-11/CFC-12 age (CFC-11/CFC-113 age will be used for after 1975) and provide an estimate of the errors resulted from these processes in the model.

Model results

The tracer fields are initialised to zero concentration on the isopycnic layers in the model. The surface boundary conditions for tritium and helium are the same as in Jia and Richards (1996), and for CFCs they are the same as in Haine and Richards (1995). The simulation is for the period 1960–1990 for tritium and helium, 1950–1990 for CFC-11 and CFC-12, and 1975–1990 for CFC-113.

Haine and Richards (1995) examined the relationships between tracer saturation levels (and hence ventilation age) and various parameterisations of the CFC surface boundary conditions, and concluded that the distribution of the oceanic mixed layer depth and its seasonal variability is the key process affecting the tracer saturations and ventilation age. The distribution of the mixed layer depth in March in the model is presented by New *et al*. (1995). It compares well with observations, with deep mixing in the high latitudes (Labrador, Irminger and Greenland–Norwegian Seas) and a typical 100–200 m mixed layer depth in the subduction zone of the subtropical gyre.

Fig. 1 shows the saturation level of CFC-113 in March 1990 in the model mixed layer. Over most of the central North Atlantic, the saturation is over 80%. It is 50% in the Labrador Sea, 40% in the Irminger Basin and 30% in the Greenland–Norwegian Seas. For CFC-11 and CFC-12, the distributions of the saturations are similar to that of CFC-113, but generally about 10% more saturated than CFC-113. Saturation of around 60% has been observed in the Labrador Sea for CFC-11 and CFC-12 (Wallace and Lazier, 1988), but Rhein (1991) reported an observed saturation level of around 80% in the Greenland–Norwegian Seas. The very low saturation level of CFCs in the Greenland–Norwegian Seas in the model may be due to the parameterisation of sea ice under which the air-sea exchange is set to zero.

As stated in the previous section, the mixed layer age derived from a CFC pair is non-zero if the pair have unequal saturations. Fig. 2 confirms that the condition of equal saturation is not met in the model for the CFCs. When all the three CFCs are undersaturated (which occurs over most of the regions in the North Atlantic in winter), CFC-113 is less saturated than CFC-11, and CFC-11 is less saturated than CFC-12 due to their different atmospheric histories and the parameterisation of their surface boundary conditions. This pattern of unequal saturation of a CFC pair, when their atmospheric ratios are used to estimate the age of water, will result in positive age in the model mixed

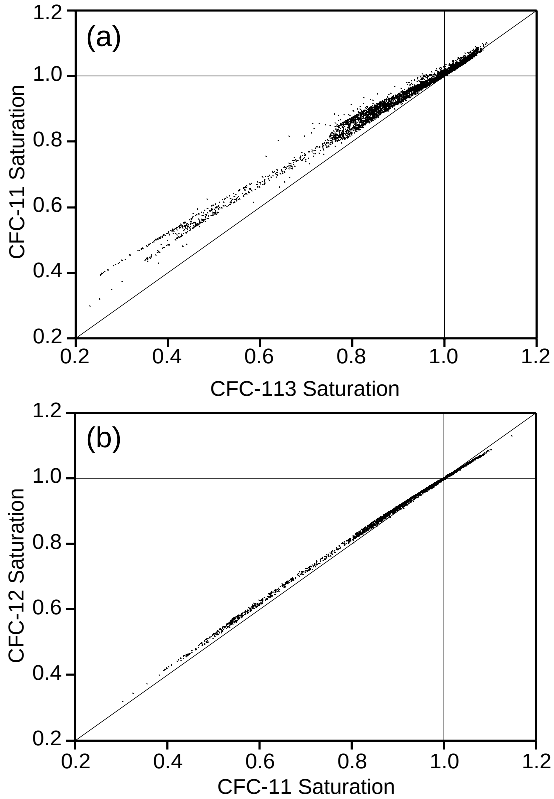

Figure 2. (a) Surface CFC-11 and CFC-113 saturations. (b) Surface CFC-12 and CFC-11 saturations. Both are computed from March 1990 of model data.

layer at winter time when subduction occurs (Fig. 3). In the region of the subduction zone of the subtropical gyre, the mixed layer age is typically 0.5–2.0 years. In the Labrador Sea, it is about 4.5 years when CFC-113/CFC-11 ratio is used (about 3.5 years when CFC-11/CFC-12 ratio is used before 1975). The greatest error is in the Greenland–Norwegian Seas where the mixed layer age reaches 9 years (7 years if CFC-11/CFC-12 ratio is used).

This positive age in the mixed layer in winter has a significant effect on the age distributions in the interior

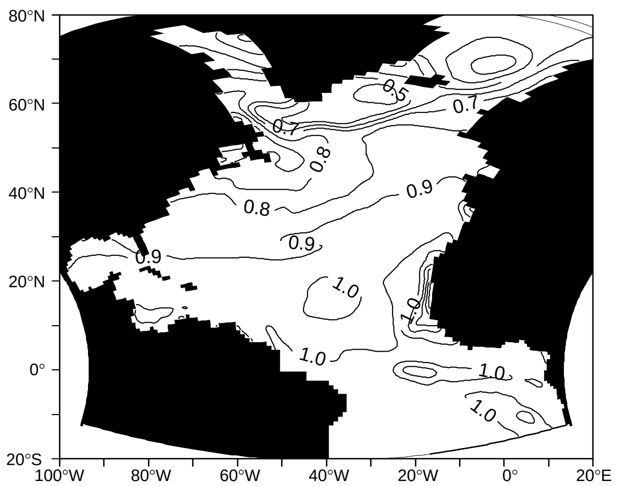

Figure 1. CFC-113 saturation in the mixed layer computed from March 1990 of model data. 1 unit = 100%.

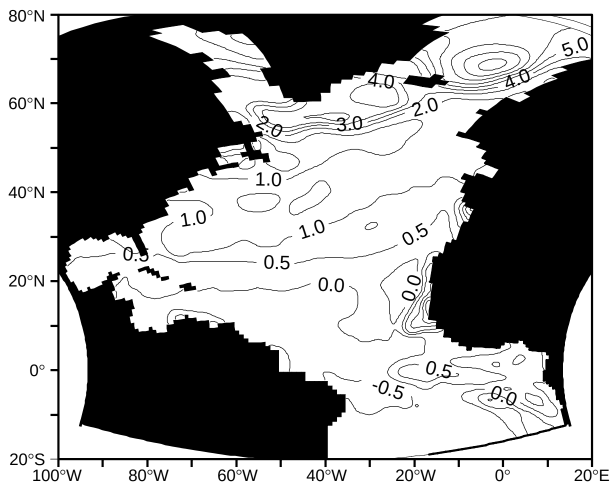

Figure 3. CFC-113/CFC-11 age distribution in the model mixed layer in March 1990. Unit: year.

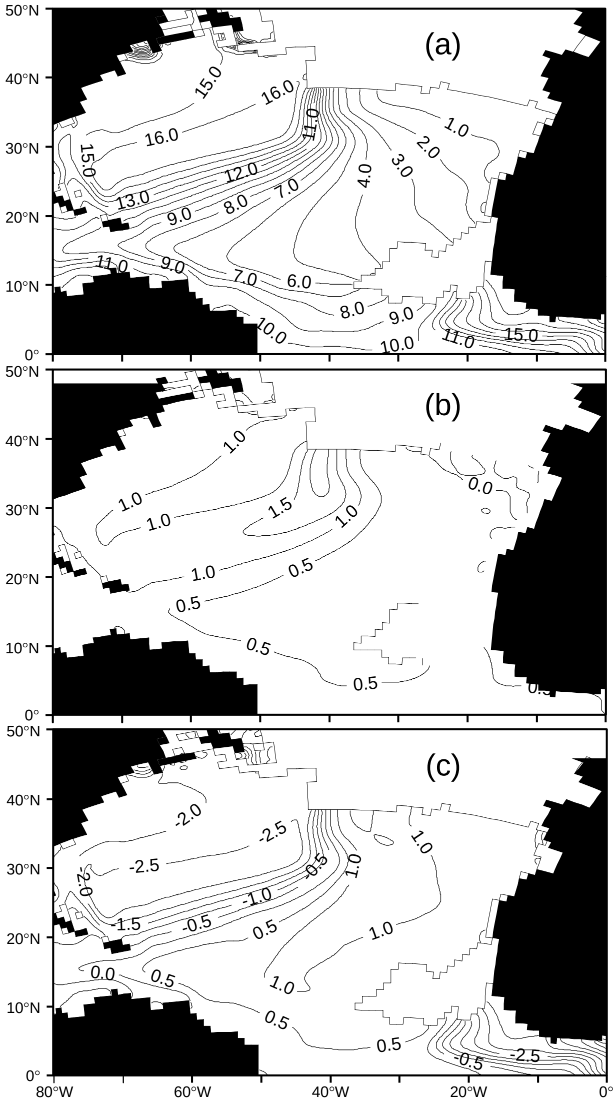

Figure 4. (a) The ideal age distribution, (b) the difference between tritium-helium age and ideal age, and (c) the difference between the CFC-113/CFC-11 age and ideal age on layer 10 ($\sigma_\theta = 26.85$) *in the model in March 1990. Age unit: year.*

isopycnic layers since it is water with these characteristics which is being subducted. Fig. 4 shows the ideal age distribution and the differences between the tracer derived ages and the ideal age on layer 10 ($\sigma_\theta = 26.85$) in the model. This layer outcrops to the mixed layer at about 40°N with maximum subduction between 30–40°W (Jia and Richards, 1996). In the ventilated region, the ideal age increases steadily from northeast to southwest with a time scale of approximately 10 years. In the pool region (where tracer can only enter through lateral isopycnic mixing), the age reaches 16 years. There is a sharp gradient between the ventilated and the non-ventilated regions (Fig. 4a).

The difference between the tritium-helium age and the ideal age on this layer ranges between 0 and 2 years (Fig. 4b), with low amplitude in the ventilated region (<1 year) and large amplitude in the area where there is a large gradient both in age and tracer concentration (Jia and Richards, 1996). This is perhaps expected since the tritium-helium age is only affected by tracer gradients associated with mixing processes. In the ventilated region, the circulation is strong in comparison with mixing (high Péclet number) and the tracer gradients are low, hence tritium-helium age is closer to ideal age.

A very different distribution is presented in Fig. 4c of the difference between CFC-113/CFC-11 age and the ideal age. The large amplitude of positive difference with a maximum of approximately 1.5 years is along the ventilation pathway (the ventilated region). This feature is purely the reflection of the surface boundary condition along the line of the outcropping of this layer to the mixed layer. The CFC-113/CFC-11 age in the mixed layer at the site of maximum subduction to this layer is around 1.5 years. In the pool region where CFC-113/CFC-11 age is least affected by the surface boundary condition but mostly affected by

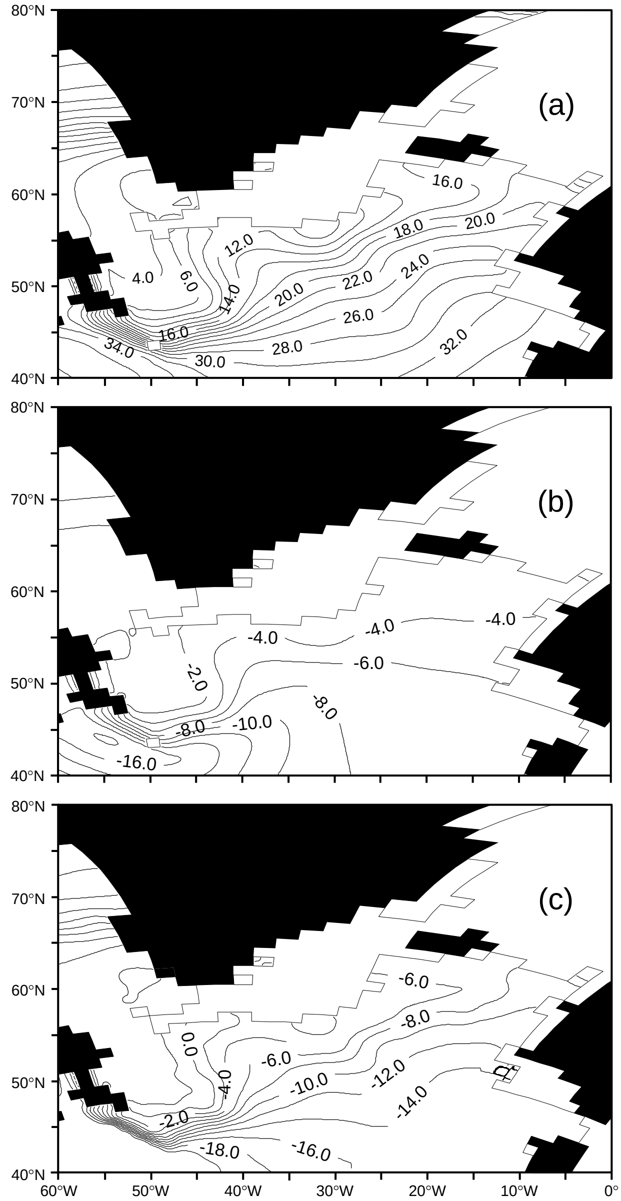

Figure 5. As Fig. 4, but for model layer 16 ($\sigma_\theta = 27.75$).

mixing processes, the difference between the CFC-113/CFC-11 age and the ideal age is negative.

The effects of non-zero mixed layer age are much greater in the high latitudes on the deeper water masses. For instance, the age of water subducted from the Labrador Sea (layer 16, $\sigma_\theta = 27.75$, Fig. 5c) will have a ventilation age of about 4 years as soon as it is isolated from the influence of the atmosphere. However, away from the subduction area, mixing processes quickly take over, which reverses the sign of the difference and results in significant under-estimate of the age of the subducted water.

In the deeper layers, the lateral (isopycnic) mixing also has a large impact on the tritium-helium age. It under-estimates the age of water on layer 16 (Fig. 5b), presumably due to the relative gradients of tritium and helium. The amplitude of the difference is large in comparison with the ideal age (Fig. 5a).

Summary

This note describes a very preliminary analysis of a simulation of CFCs with the Atlantic isopycnic model. It examines the processes affecting the tracer derived ages (tritium-helium age, CFC ages). Using ideal age as a reference, the errors resulted from these processes are estimated.

For tritium-helium age, errors result from tracer gradients associated with lateral mixing. In the mid-thermocline of the subtropical gyre, it over-estimates the age by about 2 years in the transition zone between the pool and the ventilated regions where the tracer gradients are high, it is over a year in the pool region where the Péclet number is low and it is less than 0.5 year in the ventilated region where circulation dominates. For CFC-113/CFC-11 age, lateral mixing tends to produce an under-estimate of the age, but the surface boundary condition (positive age in the mixed layer) introduces an over-estimate of the age to the main ventilated region by as much as 1.5 years near the outcropping of this layer to the mixed layer. In the interior of the gyre, lateral mixing takes over and reduces the error to zero at the western flank of the ventilated region. But in the pool region, it under-estimates the age by over 2.5 years.

For the deeper water masses (*e.g.* Labrador Sea Water), the differences between the tracer derived ages and ideal age are large. Lateral mixing tends to make both tritium-helium age and CFC-113/CFC-11 age under-estimate the ideal age, whereas the positive mixed layer age of CFC-113/CFC-11 produces an over-estimate of the age which can be traced some distance away from the subduction region.

From the above analysis, it is clear that tracer derived ages should be used with caution. If we take the ideal age as a reference for ventilation age, the tracer derived ages provide a reasonable estimate of the age of water in the subtropical gyre. For the deeper water masses, the errors are too large to give us confidence in using these tracers as a dating tool. However, a detailed analysis of the simulation is yet to be done, further investigations of the effects of lateral mixing processes and surface boundary conditions on tracer derived ages are yet to be carried out. Validation of the model results against observations is necessary before a definite conclusion can be drawn about the usefulness of the tracer derived ages.

References

Bleck, R., C. Rooth, D. Hu, and L.T. Smith, 1992: Salinity-driven thermocline transients in a wind- and thermohaline-forced isopycnic coordinate model of the North Atlantic. J. Phys. Oceanogr., 22, 1486–1505.

Doney, S.C., and W.J. Jenkins, 1994: Ventilation of the deep western boundary current and abyssal western North Atlantic: Estimates from tritium and ^{3}He distributions. J. Phys. Oceanogr., 24, 638–659.

England, M.H., V. Garçon, and J. Minster, 1994: Chlorofluorocarbon uptake in a world ocean model, 1. Sensitivity to the surface gas forcing. J. Geophys. Res., 99, 25,215–25,233.

Fine, R. A., and R. L. Molinari, 1988: A continuous deep western boundary current between Abaco (26.5°N) and Barbados (13°N). Deep-Sea Res., 35, 1441–1450.

Haine, T.W.N., and K.J. Richards, 1995: The influence of the seasonal mixed layer on oceanic uptake of CFCs. J. Geophys. Res., 100, 10,727–10,744.

Jia, Y., and K.J. Richards, 1996: Tritium distributions in an isopycnic model of the North Atlantic. J. Geophys. Res., in press.

New, A.L., R. Bleck, Y. Jia, R. Marsh, M. Huddleston, and S. Barnard, 1995: An isopycnic model study of the North Atlantic. Part 1: Model Experiment. J. Phys. Oceanogr., 25, 2667–2699.

Rhein, M., 1991: Ventilation rates of the Greenland and Norwegian Seas derived from distributions of CFMs F11 and F12. Deep-Sea Res., Part A38, 485–503.

Thiele, G., and J.L. Sarmiento, 1990: Tracer dating and ocean ventilation. J. Geophys. Res., 95, 9377–9391.

Wallace, D.W.R., and J.R.N. Lazier, 1988: Anthropogenic CFMs in newly formed Labrador Sea Water. Nature, 332, 61–63.

WOCE DIU WWW update

At the beginning of May the WOCE Data Information Unit (DIU) at Delaware rebuilt its Data Source Information Page. The most noticeable change is in the appearance of icons (disks, clipboards and globes) which make the categories on the page (data, inventories/catalogues and maps respectively) readily apparent to the user. The content continues to be updated daily.

Congratulations to the DIU for theses innovations and reader please access:

http://www.cms.udel.edu/woce/dacs.html

South Atlantic Deep Water Tracer Studies within WOCE

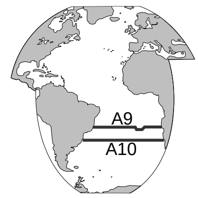

Wolfgang Roether, Alfred Putzka, Birgit Klein, Henning Rose, Christine Rüth, Jürgen Sültenfuss and Roland Well, Institut für Umweltphysik, Universität Bremen, Bremen, Germany, wroether@physik.uni-bremen.de

We have collected tracer data primarily in the South Atlantic and the Weddell Sea, mostly as a component of the German contribution to WOCE. The tracers are tritium, helium isotopes and neon, CFC-11 and CFC-12, and more lately, CCl4 and CFC-113 (Roether and Putzka, 1996). The field work is summarized in Table 1. Whereas previously much of our efforts was occupied by technical developments, sample collection and measurement, and not the least raw-data evaluation, over the years a wealth of data has become available, awaiting oceanographic evaluation. Except for tritium, and for helium isotopes/neon for the most recent cruises, all tracer data are now available at least in preliminary form. A selection of data with a very brief description is presented in the following.

Fig. 1 (page 21) shows the distribution of δ^3He for WHP sections A9 and A10 (South Atlantic, 19°S, 30°S). The structure exhibited is governed by terrigenic ^{3}He, much of which is advected from the Pacific. There is only a small contribution of tritiugenic ^{3}He in the Central Water range, and restoration toward solubility equilibrium values (about -1.7%) occurs at the air-water interface. On both sections we find rising δ^3He from the surface down to about 1000 m depth, and highest concentrations in Antarctic Bottom Water (AABW), west of the MAR on A9, and on A10 everywhere except in the Angola Basin (14°W–2°E). Lower concentrations in between reflect the North Atlantic sources (NADW). On A10 one notes an inclined minimum layer with rather low values in the deep Angola Basin, proving substantial addition of NADW to the latter; slightly higher bottom concentrations toward the Walvis Ridge indicate leakage of high- δ^3He water from the Cape Basin. Further features are a pronounced signature of upper NADW on A9 (appr. 1800 m) but much less so on A10, and local maxima near the ridge crest of the MAR on both sections, but with a reversed prominence relative to that of upper NADW. The extended mid-depth δ^3He maximum on A10 must be ascribed either to the presence of Circumpolar waters, or to local sources on the MAR. The latter explanation is supported by high δ^3He / silica ratios accompanying this maximum (Fig. 2), which exceed those in AABW and other ACC waters by up to a factor of 2. The example of Figs. 1 and 2 demonstrates a potential of ^{3}He as a steady-state water mass tracer (Roether *et al.*, 1996).

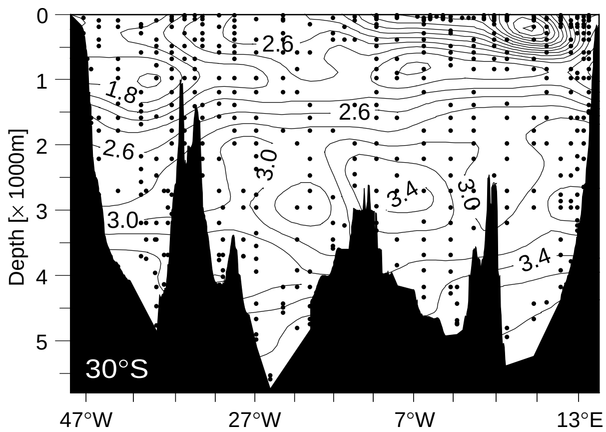

Figure 3. Neon (% deviation from solubility equilibrium) along WOCE section A10 (see Figs. 1b, 2).

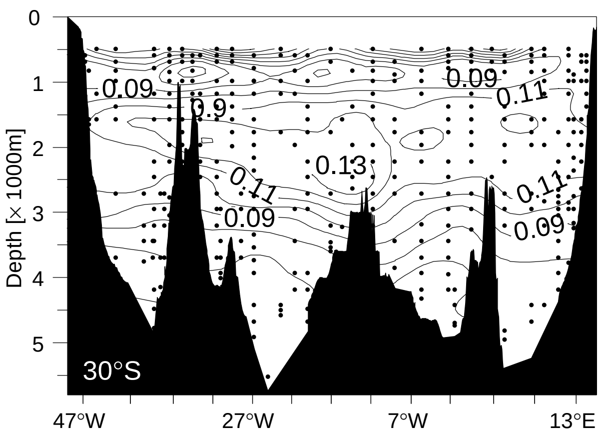

Figure 2. δ^3He to silica ratio (%/(mmol/kg)) for WOCE-WHP section A10 (see Fig. 1b).

Fig. 3 shows a neon section for A10. Neon has no inner-ocean sources, and therefore the oceanic concentrations are comparably more uniform, which makes measurement even more critical (our achieved precision is appr. ±0.35%). The primary purpose of our neon measurements has been to assist in the separation of inner-ocean sources for the helium isotopes (see above), but to our surprise we found significant structures also in the neon distributions. A particularly interesting feature are minimum concentrations (less that 2% in DNe) in Antarctic Intermediate Water (AAIW), which we find consistently in all our data. Low neon concentrations arise from a combination of low atmospheric pressure, and a relative absence of breaking waves, during AAIW formation. The conditions must differ significantly from those for NADW and AABW formation, which both exhibit higher neon values. We therefore expect clues on AAIW formation from the neon data.

The last example refers to the more common group of transient tracers, the CFCs and CCl_4, and to a different WOCE section, A8 at 11.8°S. The CCl_4 distribution on A8

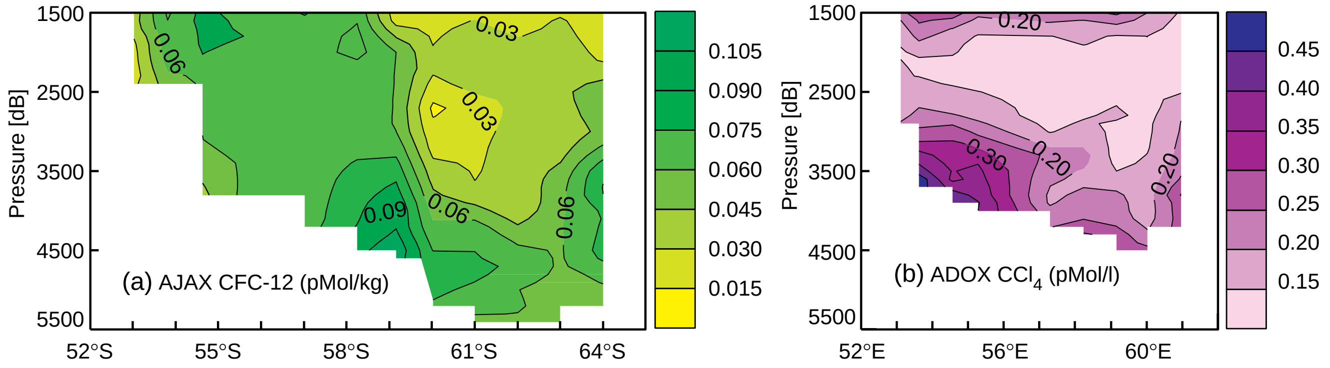

Haine, page 3 *Figure 1. (a) Dissolved CFC-12 concentration (pmol/kg) in 1982 on the AJAX section (Weiss et al., 1990). (b) Dissolved* CCl_4 *concentration (pmol/l) in 1993 on the ADOX section between Crozet and Kerguelen.*

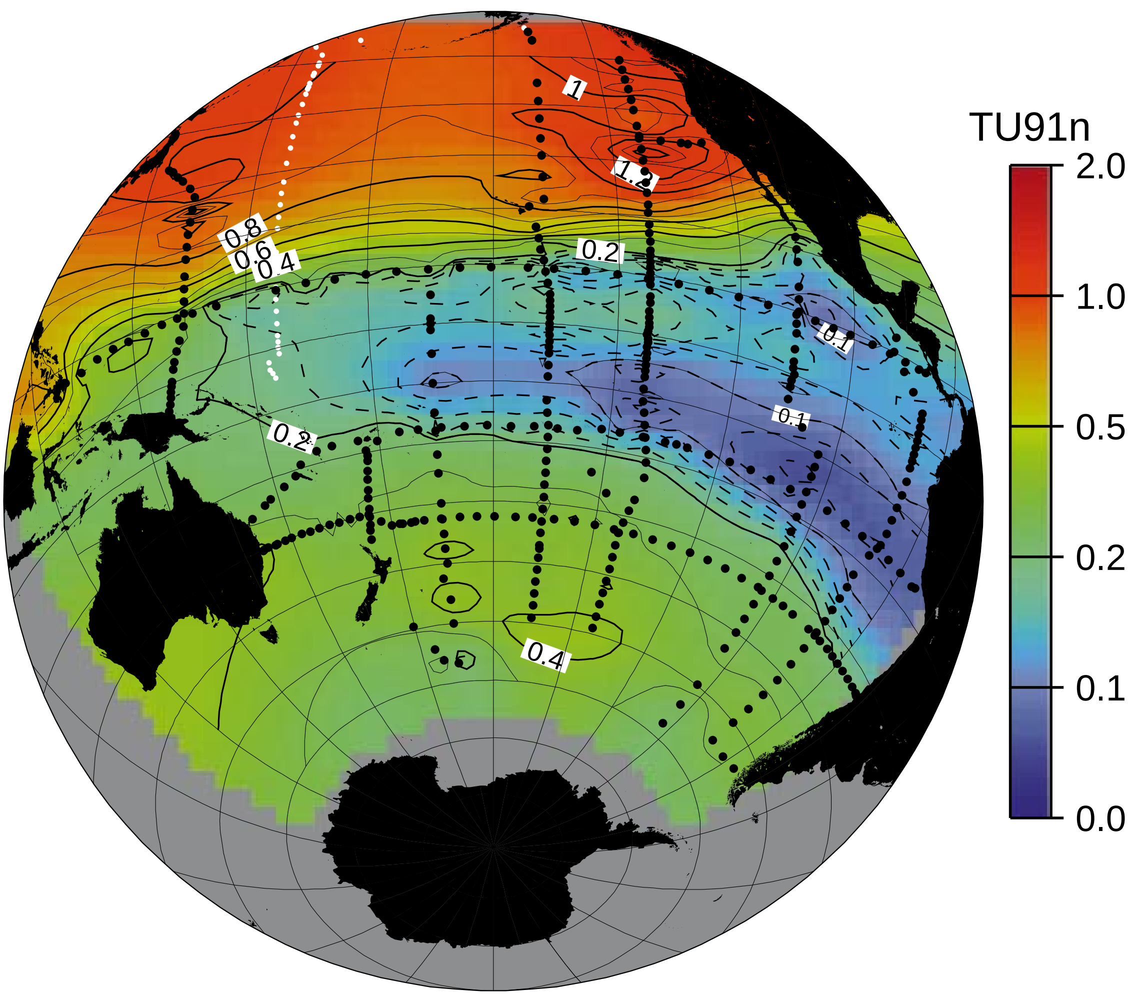

Jenkins, page 8 *Figure 4. The distribution of tritium (in TU) on the 26.8 kg/m*^{3} *potential density anomaly surface in the Pacific. The black dots are station locations used in mapping the tritium. The white dots are stations sampled but not yet analyzed. Note the double tongue of low tritium water in the eastern tropical Pacific.*

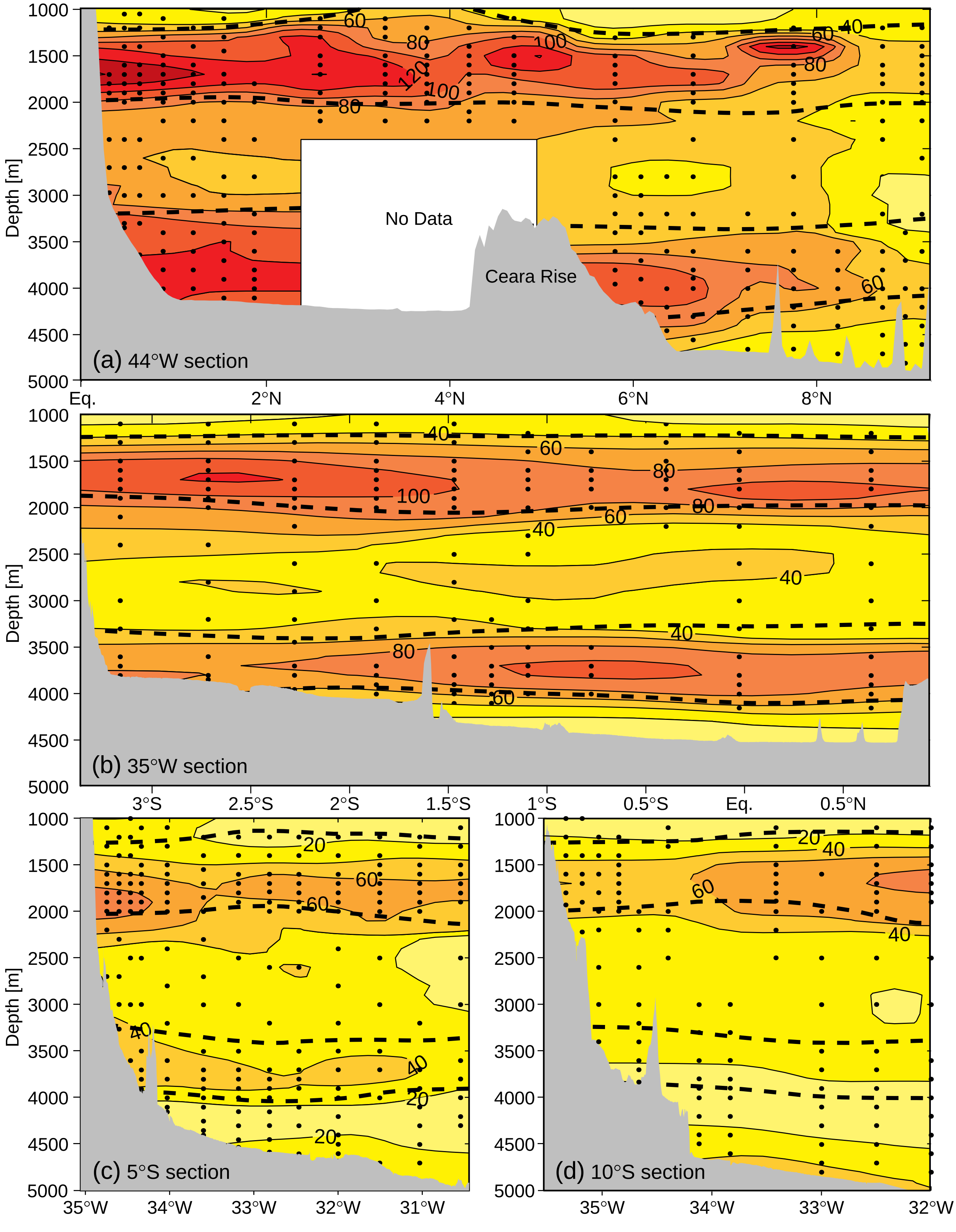

Rhein et al., page 12 *Figure 2. CFC-11 sections in* 10^{-15} *mol/kg, depth range below 1000 m (a) at 44°W, (b) at 35°W, (c) at 5°S and (d) at 10°S. The dashed lines represent the isopycnals* $\sigma_{1.5}$ *34.45 and 34.70,* σ_4 *45.83 and 45.90, which were chosen by Rhein et al., 1995 as the boundaries for the SUNADW and OLNADW.*

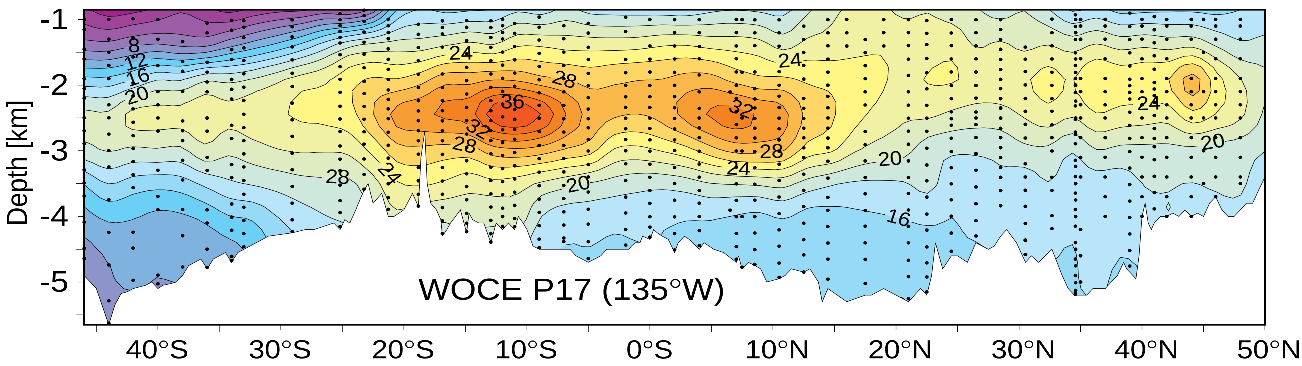

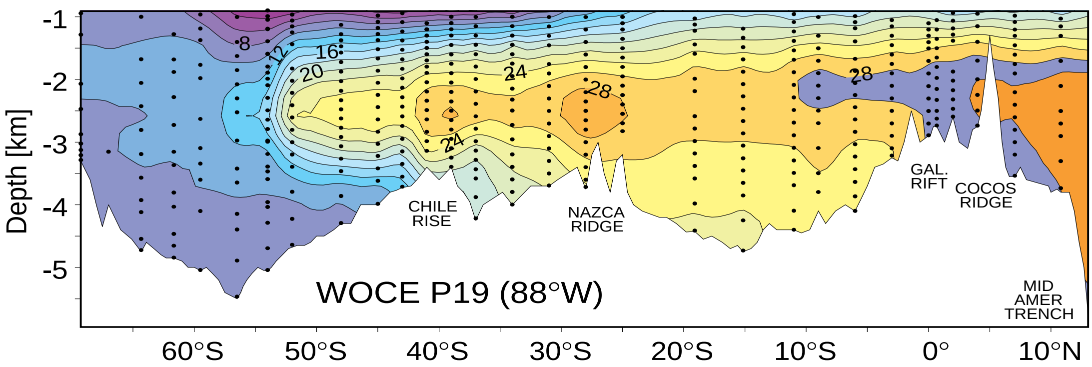

Lupton, page 9 *Figure 2. δ^3He% contoured along WOCE sections P17 and P19 from 1000 m depth to the bottom. δ^3He is the percentage deviation of the $^3He/^4He$ ratio from the ratio air. Precision of the measurements is about $1\sigma = 0.2\%$ in δ^3He. Contour interval is 2%.*

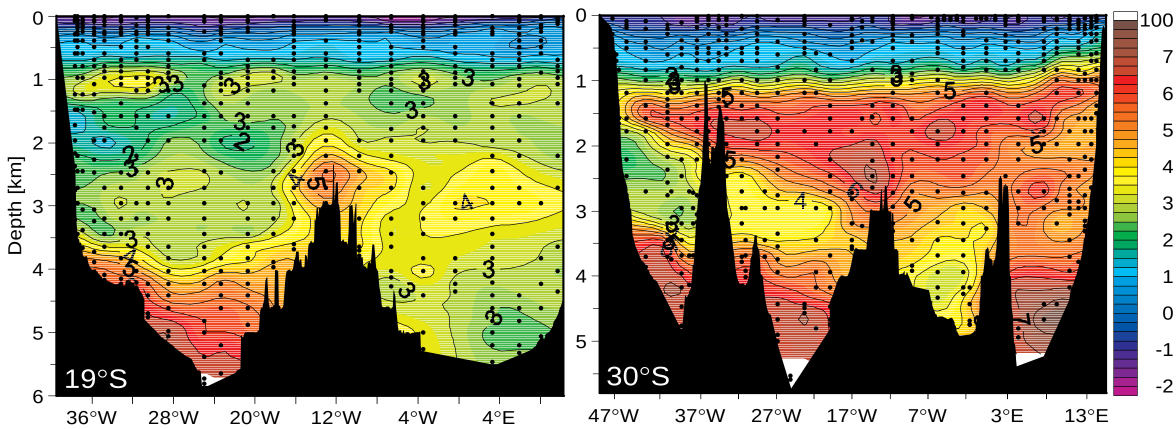

Roether et al., page 18 *Figure 1. δ^3He (% deviation from atmospheric $^3He/^4He$ ratio) along WOCE sections A9 at 19°S; left panel and A10 at 30°S; right panel. Dots indicate the location of data points, measurement precision is approximately ±0.25%.*

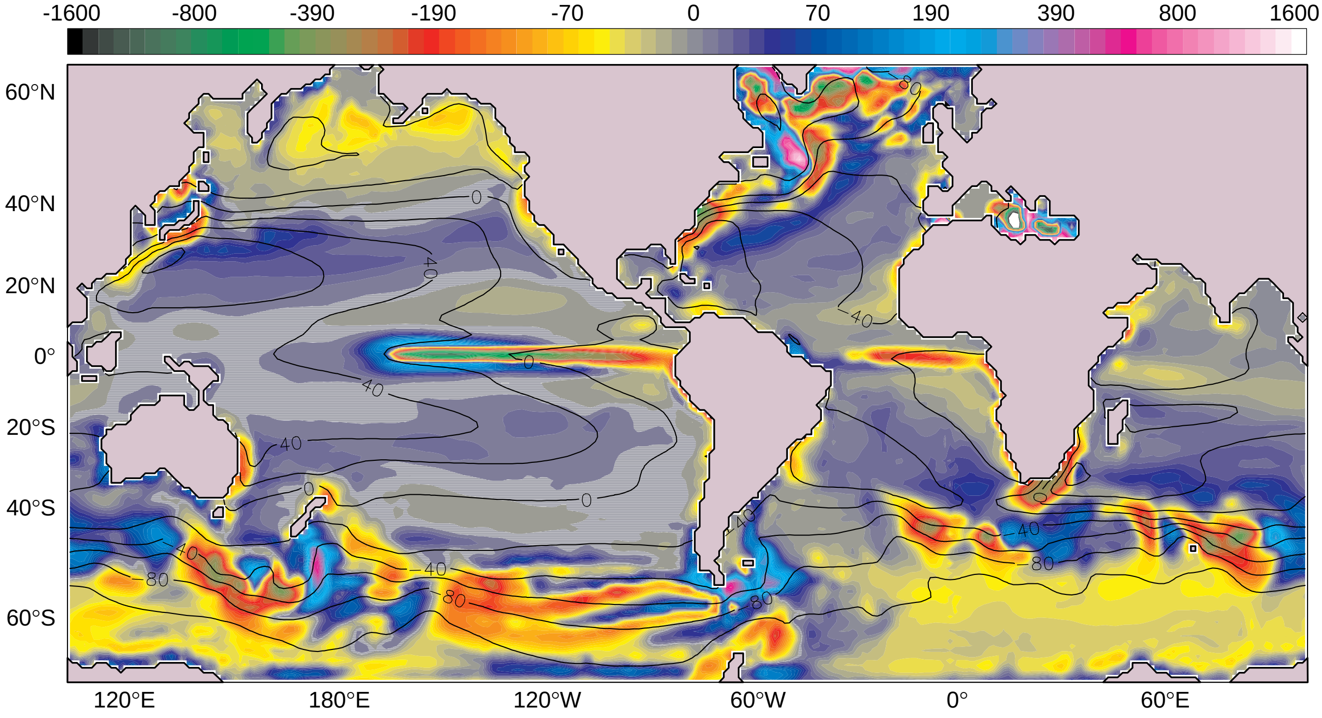

Bleck, page 32 *Figure 2. Vertical mass flux (m/yr) through bottom of mixed layer, averaged over years 70–75. Positive numbers indicate downward motion. Note exponentially expanding contouring interval. Sea-surface height contours added to indicate surface flow. Contour interval: 20 cm.*

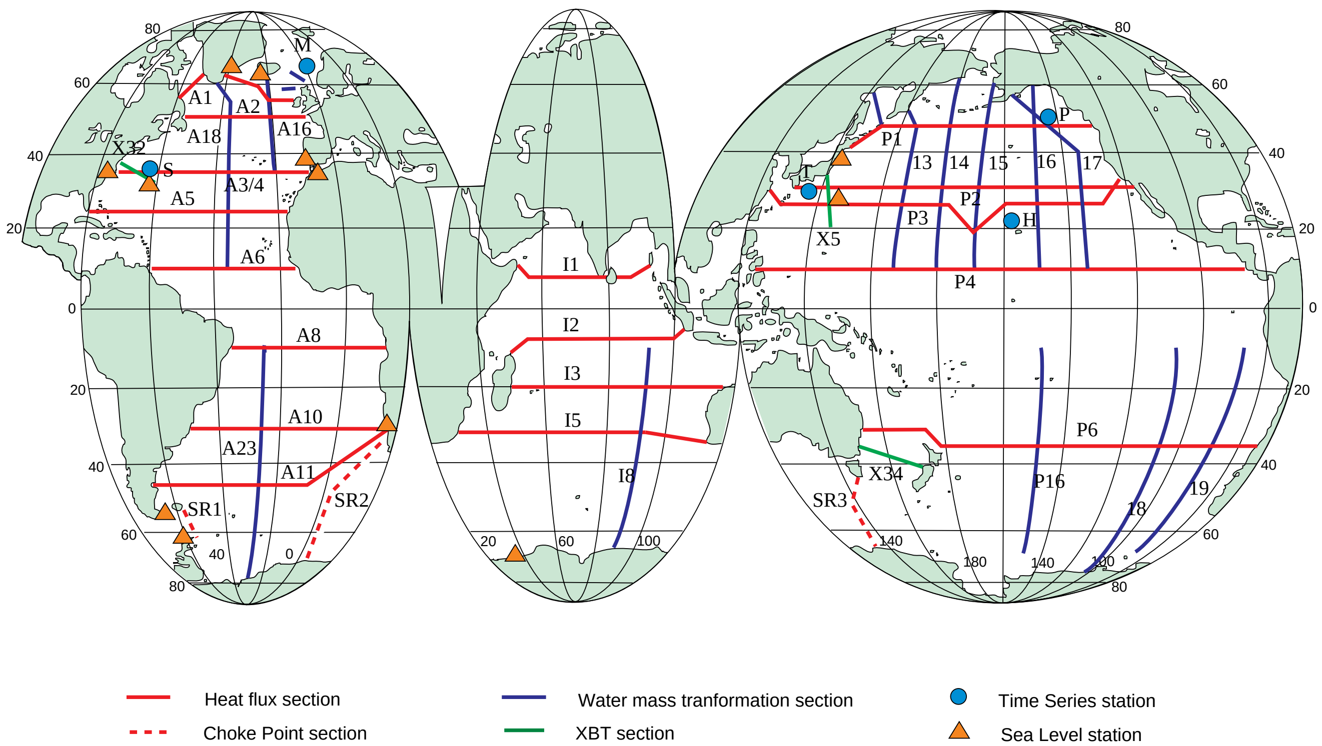

Gould, page 38 *Possible WOCE measurements to be continued under CLIVAR.*

(Fig. 4) gives particularly clear evidence of the advective cores of NADW and AABW adjoining the western boundary of the South Atlantic, especially the uNADW is very prominent along the section and extends up to the MAR. CCl_4 concentrations decrease gradually eastward, towards low or undetectable values in the vicinity of the eastern boundary (oldest waters centred around 3000 m depth). We find that CCl_4 is considerably more sensitive to detect small contributions of younger water in very old waters than it is the case for the more common CFCs, *i.e.* CFC-11 and CFC-12. At the bottom of the eastern basin the increase of concentrations indicates admixtures of younger waters. A special feature is the CCl_4 minimum in the Central Water range (appr. 300 m), which is due to upper-ocean decomposition. We find however that decomposition hardly imparts the usefulness of CCl_4 as a transient tracer in the deep, cold waters of the ocean (Wallace *et al.*, 1994).

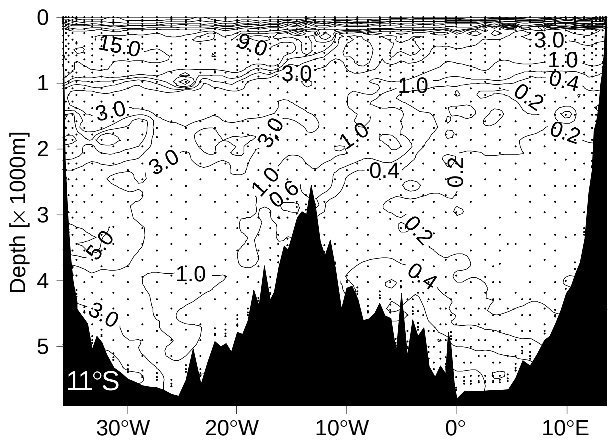

Figure 4. CCl_4 partial pressure (pptv) along WOCE section A8 at 11.8°S.

Table 1: Summary of the field work conducted by the tracer group in Bremen

Tables: Cruise	Section	Samples
M11/5	A21 S4 A12	CFC, He, T
M15/3	A9	CFC, He, T
M18	A1-West	CFC
ANT X/4	A12	CFC, He, T
M22/5	A10	CFC, He, T
M28/1	A8	CFC, He, T
M30/2	A2	CFC
Cither3-1	A14	He, T
Cither3-2	A13	He, T
JCR 10	A23	He, T
ANT XIII/4	A12, S4	CFC, He, T

Acknowledgements

We acknowledge funding by BMBF, DFG and Univ. Bremen (FNK). The assistance of our technical staff and various students is appreciated. We are grateful to Prof. Siedler and Dr Fahrbach and the crews of Meteor and Polarstern for their cooperation during the cruises.

References

Roether, W., R. Well and A. Putzka, 1996: Component separation of oceanic helium. J. Geophys. Res., in revision.

Roether, W., and A. Putzka, 1996: Transient tracer information on ventilation and transport of South Atlantic Waters, in 'The South Atlantic: Present and Past Circulation', G. Wefer, W.H. Berger, G. Siedler, D. Webb, Eds., in press.

Wallace, D.W., P. Beining, and A. Putzka, 1994: Carbon tetrachloride and chlorofluorocarbons in the South Atlantic Ocean, 19°S, J. Geophys. Res., Vol. 99, 7803–7819.

Assimilation of CFC Data into an Ocean Circulation Model

Reiner Schlitzer, Alfred-Wegener-Institut für Polar- und Meeresforschung, 27515 Bremerhaven, Germany, rschlitzer@AWI-Bremerhaven.de

Chlorofluorocarbons (CFCs) are a group of man-made substances that have been released to the atmosphere in increasing amounts during the last few decades and have invaded the ocean since then. These substances are easy and cheap to measure, and CFC observations have become an integral part of the WOCE hydrographic programme. CFCs are relatively stable compounds, they enter the surface waters of the ocean by gas-exchange and are then transported into the interior by ocean circulation and mixing processes. In general, CFC concentrations are highest in cold polar and subpolar surface waters and small in the deep ocean. However, in areas of deep reaching convection and deep-water formation, large amounts of CFCs are transported to great depths and are then distributed along the pathways of intermediate-, deep- and bottom-water masses. Because of zero natural CFC background concentrations, the flow of these water masses can be traced by tongues of CFC-enriched water that evolve in time.

Using repeated CFC observations, the spreading of the sub-surface water masses can be monitored, however, in order to quantify these flows, the use of CFC-calibrated circulation models is required. Because traditional inverse models that deduce transport rates directly from data can not be applied for the CFCs due to sparseness of data in space and time, there is a need for new ocean circulation models that are specifically adapted to the characteristics of

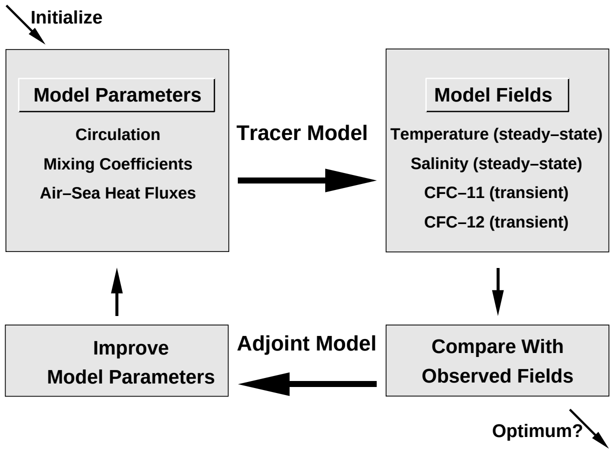

Figure 1. Schematic flow chart showing the individual steps of the optimization procedure. Note that the comparison between simulated model fields and observations as well as the subsequent parameter improvements are performed automatically by the adjoint method.

CFCs and transient tracers in general. Here, I present a new strategy that aims at obtaining information on large-scale, mean water mass transport rates by fitting a circulation model to CFC and hydrographic data. As will be described below, this model consists of an iterative optimization scheme for the model circulation which, in order to be used on present day computers for basin-scale or global models, requires a restriction to steady model flows on a relatively coarse spatial model grid (coarse compared to modern, eddy-permitting dynamical models but fine compared to traditional box models). Improvements in computing hardware will allow higher resolution and time-varying flows in future versions of the model.

Strategy

Fig. 1 shows the individual steps involved in the overall model optimization procedure. Given a set of model parameters (the initial flow field is obtained from geostrophic calculations using the historical temperature and salinity data-base, mixing coefficients and air-sea fluxes are taken from the literature) and boundary values at open-ocean boundaries of the model, a tracer model is used to derive simulated CFCs distributions and hydrographic fields inside the model domain. The tracer model conserves mass, heat, salt and CFCs exactly and it predicts steady (long-term mean) model fields for temperature and salinity and time-varying distributions for CFCs. While this so-called forward step is following a conventional approach, the subsequent backward step or “learning phase” is new. Traditionally this learning phase is performed manually: the comparison of simulated and measured fields is done visually and possible causes for model misfits as well as supposed improvements to the model flows are derived on the basis of subjective reasoning. Experience has shown that this process is tedious for large, complex models and that success is not guaranteed (in most cases the new simulations using the modified flows come out to be worse than the previous ones).

At this point the adjoint method (Thacker, 1988; Schlitzer, 1993) comes to a rescue. The evaluation of model-data misfits is performed automatically as part of the model calculations and the information contained in these deviations is converted into corrections for the model parameters. The numerical cost of the adjoint-step is comparable to the cost of the forward run and, most importantly, the new, modified set of model parameters (flows, etc.) is guaranteed to produce more realistic property simulations. One cycle consisting of a forward and its associated adjoint run completes one iteration of the optimization. Running this cycle repeatedly will eventually result in a (local or global) minimum for the misfits and thus yield a model circulation that produces best possible CFC and hydrographic fields. Note that in addition to considering property misfits, the adjoint step also takes into account dynamical principles and smoothness constraints (Schlitzer, 1993).

Results

Although the model scheme described above is specifically designed to fit a circulation model to hydrographic and transient tracer data, it is not clear from the beginning how close the final, optimal model state will reproduce the observed fields. Using CFC observations from the northeast Atlantic (Doney and Bullister, 1992) and corresponding model CFC values, I show in Fig. 2 that the numerical procedure works efficiently and that the optimal model CFC distribution explains the observations well.

The distribution along a meridional section at about 23°W in the northeast Atlantic (Fig. 2a) is typical for oceanic CFCs: (1) concentrations are highest near the surface with warm waters showing lower CFC levels compared with cold surface waters; (2) concentrations decrease rapidly with depth in tropical and subtropical areas whereas in regions close to convection and deepwater formation areas appreciable CFC concentrations are found throughout the water column; (3) the spreading of subsurface waters leaves signatures in the CFC distribution as indicated, for instance, by the southward extension of the 1 pmol/kg isoline in about 1500 m depth at 45°N.

The model simulated CFCs obtained using an initial flow field are shown in Fig. 2b. It is obvious that although some large-scale features of the CFC data are recovered (*e.g.*, high concentrations near the surface increasing towards colder temperatures, high CFC values in the depth range of the southward spreading North Atlantic Deep Water (NADW)) there are significant model-data misfits especially in the upper 1000 m of the water column north of 40°N. The overall agreement between simulation and observation is poor.

Starting with these fields the optimization procedure of Fig. 1 has been applied and several thousand iterations have been performed until the algorithm indicated that a minimum was reached. Fig. 2c shows the resulting CFC distribution for the optimized model state. The model CFC field has been significantly modified in the course of the optimization and is now in close qualitative and quantitative agreement with the observations: (1) the CFC-11 distribution in the main thermocline is now modeled realistically, (2) the downward penetration of CFC in the tropical region has been reduced and (3) the southward spreading of NADW has been adjusted in order to obtain close resemblance of CFC data for depths greater than 1000 m.

The close agreement between simulation and data that has been described for the Oceanus 202 section is also found in other areas of the model domain and for other time periods. Having shown that a steady flow field which is consistent with geostrophic shear estimates obtained from hydrographic data (Schlitzer, 1996) can closely reproduce the measurements, the next step is to analyze and characterize the circulation pattern capable of doing this. This analysis is underway and results on water mass transports and diagnosed air-sea CFC fluxes will be presented in an upcoming paper.

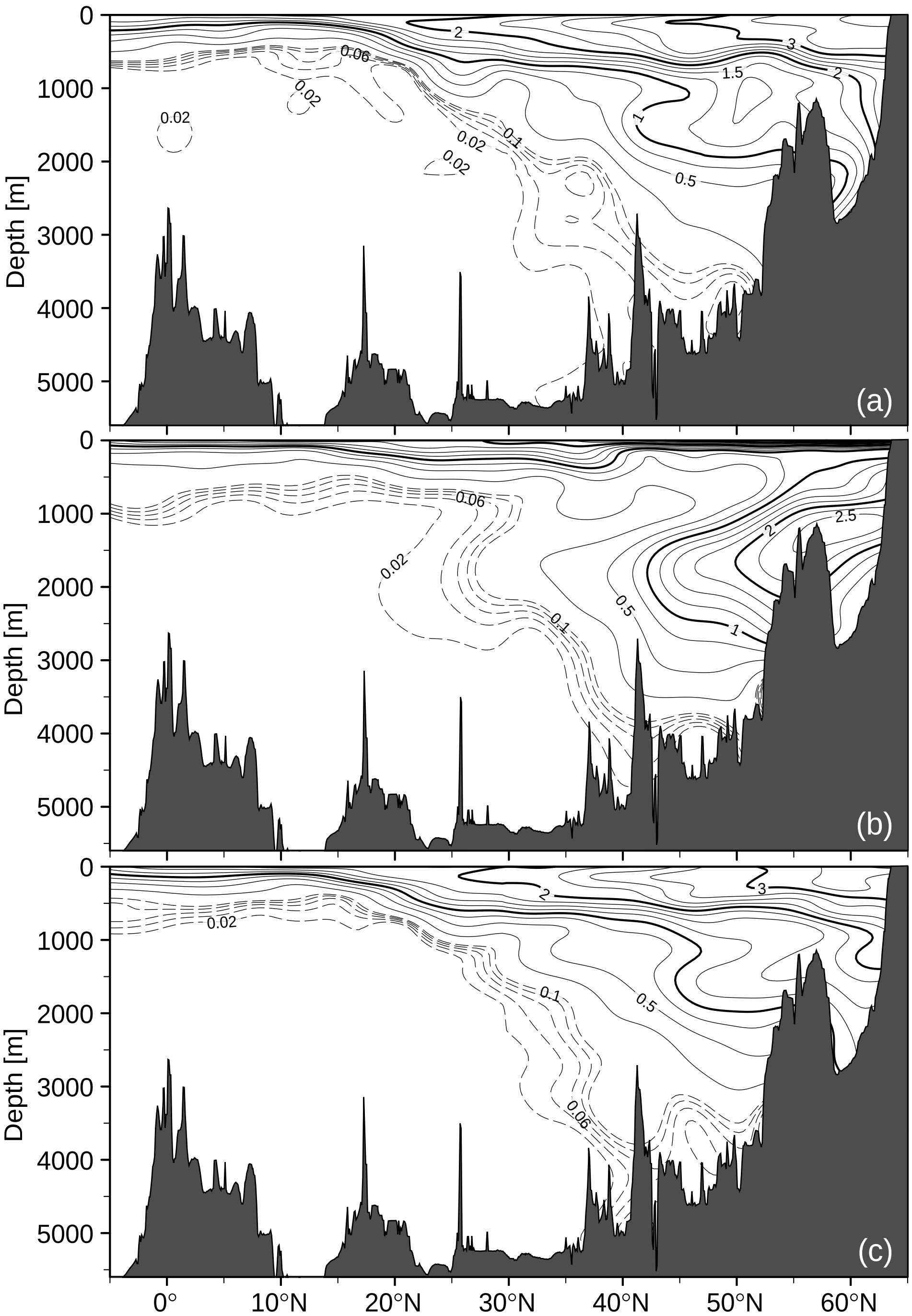

Figure 2. Distribution of CFC-11 (pmol/kg) along the track of Oceanus cruise 202 (northeast Atlantic, about 23°W) (a) data redrawn from Doney and Bullister (1992), (b) model simulation using the initial model flows and (c) model simulation based on the final, optimized model flows.

References

Doney, S.C., and J.L. Bullister, 1992: A chlorofluorocarbon section in the eastern North Atlantic. Deep-Sea Res., 39, 1857–1883.

Schlitzer, R., 1993: Determining the mean, large-scale circulation of the Atlantic with the adjoint method. J. Phys. Oceanogr., 23, 1935–1952.

Schlitzer, R., 1996: Mass and heat transports in the South Atlantic derived from historical hydrographic data. In: The South Atlantic: Present and Past Circulation, G. Wefer, W.H. Berger, G. Siedler, D. Webb (eds), Springer, Heidelberg.

Thacker, W.C., 1988: Three lectures on fitting numerical models to observations. Report GKSS 87/E/65. GKSS Forschungszentrum, Geesthacht.

Acknowledgements

The author would like to thank R.F. Weiss, W.M. Smethie, W. Roether, J.L. Bullister, A. Poisson and M. Rhein for letting me use their CFC data for the model assimilation runs.

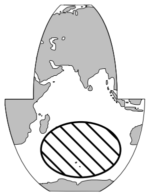

On the Distribution of Bomb Carbon-14 in the Southern Ocean

Joachim Ribbe and Matthias Tomczak, The Flinders University of South Australia, School of Earth Sciences, GPO Box 2100, Adelaide 5001, Australia; and Claudio Tuniz, Australian Nuclear Sciences and Technology Organisation, PMB 1, Menai, NSW 2234, Australia, mojr@es.flinders.edu.au

In an earlier WOCE newsletter (Ribbe and Tomczak, 1995) we reported on the development of an off-line radiocarbon validated tracer model for the Southern Ocean based on the Fine Resolution Antarctic Model (FRAM). During the initial stages of the project computational experiment were carried out with the model for an idealised oceanic tracer. We intended to verify the physical mechanisms that operate in the model and are responsible for removing atmospheric tracer and surface water. The results of these experiments have recently been reported in a series of papers (Ribbe and Tomczak, 1996a, 1996b, 1996c) and some very early results were published in this newsletter previously.

In this note we report on the first experiments to investigate the uptake of bomb carbon-14 within the model. The effect of convection has been quantified in one of our experiments shown here. The integrated bomb carbon-14 flux due to convection alone results in an oceanic uptake of approximately 15%. We are presently investigating the sensitivity of the total uptake to effects such as changes in fluxes at the northern model boundary, the distribution of convection, and sea-ice coverage.

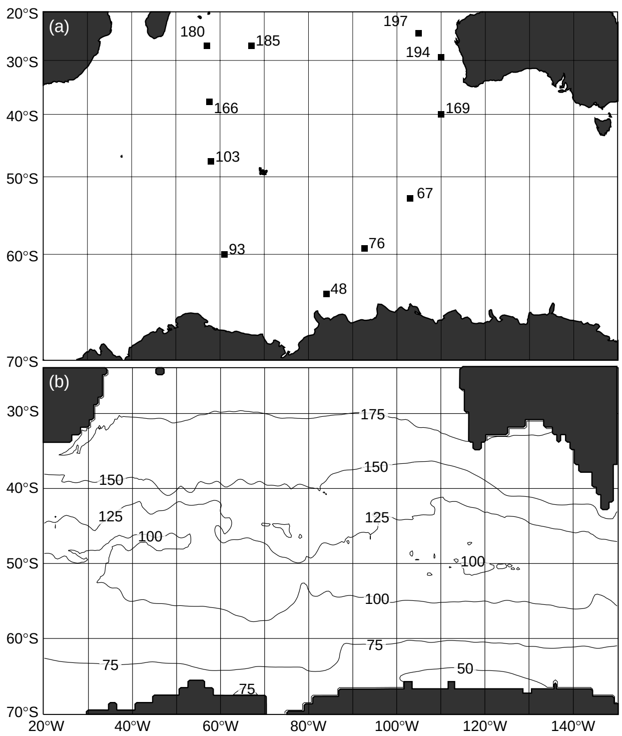

Figure 1. Distribution of bomb carbon-14 [ppt]: (a) as derived from observations (Broecker et al., 1995), and (b) as calculated by the tracer model for the Indian Ocean and the year 1978.

Although the model covers the ocean area south of 24°S, the discussion in this note is limited to bomb carbon-14 in the Indian Ocean. This ocean has been the focus of our earlier communications, which dealt with the formation of Subantarctic Mode Water (SAMW) in the southeast Indian Ocean. Our intention with the model is to quantify the role of this process for bomb carbon-14 uptake. During the last few months we were able to analyse samples collected from the Great Australian Bight (GAB) for carbon-14 using, for the first time in Australia, the Accelerator Mass Spectrometry (AMS) technique (Ribbe *et al.*, 1996). The model will eventually be applied to interpret the distribution of carbon-14 within the Australian sector of the Southern Ocean where a radiocarbon sampling programme is being carried out along WOCE Sections SR3 and SR4.

Method

The methodology in setting up the tracer model was described in Ribbe and Tomczak (1995). The same approach is taken here in our bomb carbon-14 experiments. The bomb carbon-14 is added to the model following the approach of Duffy *et al.* (1995). We are using a wind-dependent exchange coefficient calculated from the FRAM wind field. The atmospheric carbon-14 history for the southern hemisphere is taken from Vogel and Marais (1971). At the northern boundary bomb carbon-14 values are prescribed for inflowing water using the time history of carbon-14 values in surface water given by Broecker *et al.* (1985).

Carbon-14 values are reported as D14C in [ppt] which is the deviation of the 14C/12C ratio from a standard value of that ratio. The guidelines for ocean water samples were laid out by Stuiver and Polach (1977). We followed the same procedure but will refer to D14C as a carbon-14 concentration. Various properties are calculated for the modelled bomb D14C distribution; our values for the bomb carbon-14 inventory, the mean penetration depth, mean surface value and mean column inventory should be compared to the data presented in Duffy *et al.* (1995) and Broecker *et al.* (1995).

Results

The evaluation of both the modelled and observed data is in a very early stage and we would like our results to be considered as preliminary.

In Fig. 1 we show the bomb carbon-14 distribution calculated by the model in a comparison with the bomb carbon-14 data calculated by Broecker *et al*. (1995) from GEOSECS Indian Ocean observations. The agreement between both data sets is generally quite reasonable with observations (Fig. 1a) and modelled data (Fig. 1b) closest north of 30°S. The modelled data clearly show the observed north-south gradient with the lower values in the south. The gradient is a result of the surface Ekman transport which removes surface water and introduces tracer quantities to the north.

The area of SAMW formation in the southeast Indian Ocean, located in the model between 100° to 130°E and 45° to 55°S, is characterised by minima in the bomb carbon-14 distribution with values below 100 ppt. Mid-latitudinal convection removes the bomb carbon-14 signal from the surface and homogenises the water column down to a depth of 300–400 m.

The mismatch between the observed and modelled data might be related to the presentation of physical mechanisms in the model, the procedure used by Broecker *et al*. (1995) to calculate the bomb-carbon-14 signal or a combination of both. It is worthwhile to notice that Duffy *et al*. (1995) used various approaches to model the distribution of bomb carbon-14 in global ocean models and obtained surface maximum carbon-14 values within the centre of the south Pacific Ocean gyre ranging from 180 ppt to 330 ppt. The exact causes for the mismatch between observations and our model require further analysis.

Several surface water samples collected within the Great Australian Bight were recently analysed using the AMS technique (Ribbe *et al*., 1996). The observed values are in the range of 84–101 ppt (Fig. 2a) which compares to model values in the order of 100 to 125 ppt. The model integration was carried out for the bomb carbon-14 signal only, and in the absence of the natural carbon-14 component a discrepancy is expected. However, north of the Subantarctic Front which in the south east Indian Ocean is located at approximately 42°S, surface carbon-14 values are dominated by the bomb carbon-14 signal.

While the data shown in the previous figures concentrated upon the situation in the south east Indian Ocean, we will look in the following into the temporal evolution of the 'global' bomb carbon-14 integral. We calculated the total model bomb carbon-14 inventory (Fig. 3a), the mean penetration depth (Fig. 3b), the mean surface value (Fig. 3c) and the mean column inventory (Fig. 3d) for three experiments. In experiment 1 (solid line), no southward flow of bomb carbon-14 across the northern model boundary was specified. The inventory was solely determined by atmospheric input. In experiment 2 (long dashed line), a boundary

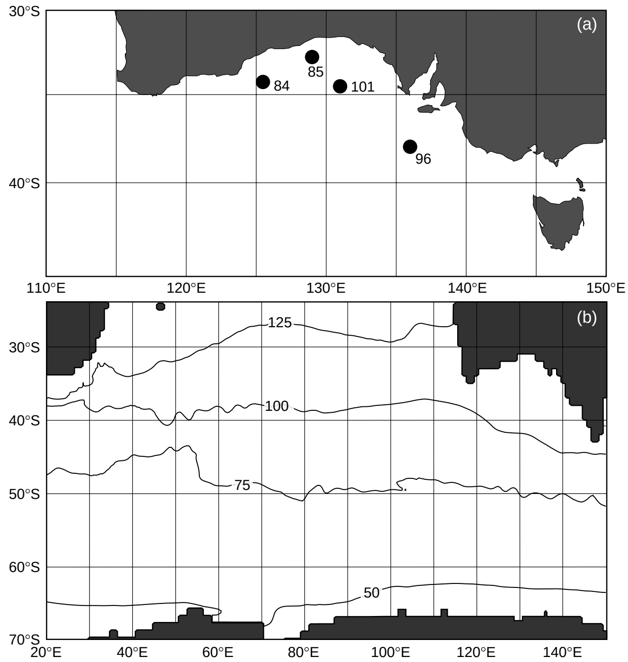

Figure 2.(a) Distribution of observed carbon-14 [ppt], and (b) of bomb carbon-14 calculated by the tracer model for the Indian Ocean and the year 1994.

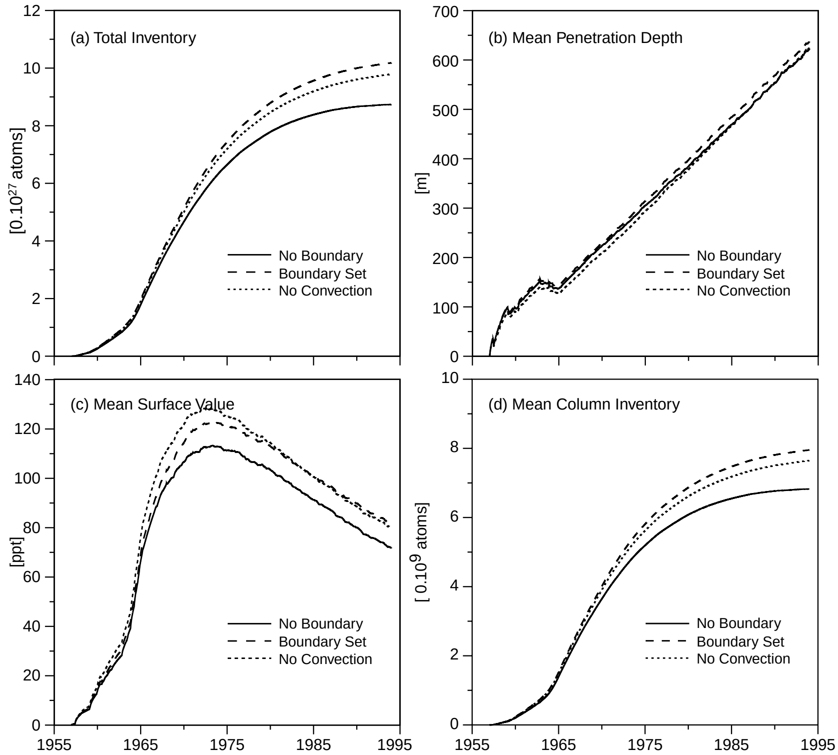

Figure 3. (a) Total bomb carbon-14 inventory [atoms] for the area of the Southern Ocean south of 24°S, (b) mean penetration depth [m], (c) mean surface value [ppt] and (d) mean column inventory [atom]. In each graphic the results of three model experiments are presented: integration for atmospheric input without specified northern boundary (NBD) inflow (solid line), integration for atmospheric input with NBD inflow specified (long dashed line), and integration for atmospheric input with NBD inflow but no convection (short dashed line).

flow was specified in addition to atmospheric input and in experiment 3 (short dashed line) we switched off oceanic convection but maintained both boundary and atmospheric input. Broecker *et al*. (1995) estimated a total inventory of approximately $5.4 \cdot 10^{27}$ atoms and a specific water column inventory of $8 \cdot 10^{9}$ atoms / cm^{2} for the ocean area south of 20°S and observed during GEOSECS. This compares with our values of $6.5 - 7.5 \cdot 10^{27}$ atoms for the total inventory (Fig. 1a) and a mean column inventory of $5.0 - 5.5 \cdot 10^{9}$ atoms / cm^{2} in 1975. The mean surface value and the mean penetration depths of bomb carbon-14 observed during GEOSECS for the global ocean are given with 155 ppt and 391 m by Broecker *et al*. (1995) and with approximately 170–190 ppt and 250–320 m by Duffy *et al*. (1995). We obtained values of 110–125 ppt and 280–300 m, which is lower than the values obtained by Broecker as well as Duffy. This is expected, as the Southern Ocean is dominated by upwelling and northward Ekman transport associated with flow out of the model domain.

In our model experiments, we are particularly interested in the effect of the convection parameterisation. This effect can be quantified by integrating the model without convection which results in a reduced oceanic uptake of bomb carbon-14 by approximately 15%. To describe in detail the parameterisation and distribution of convection in the model is beyond the intent of this note, but further details can be obtained from our manuscripts submitted for publications (Ribbe and Tomczak, 1996a, 1996b, 1996c) or by contacting us directly.

Conclusion

In an earlier note we described our plans with the development of the Southern Ocean tracer model. This progress report shows that our first results are in good agreement with work done previously, both by observationalists and modellers. The overall good agreement of modelled and observed data allows us to draw some preliminary conclusions on the effects of oceanic convection on bomb carbon-14 uptake. Some data mismatches still remain to be explained and minimised in further model development.

Acknowledgment

Dr D. Stevens at the University of East Anglia in England was an invaluable source of information; he supplied many FRAM data and assisted throughout the project. We thank him for his genuine support.

References

Broecker, W.S., T.-H. Peng, G. Ostlund. and M. Stuiver, 1985: The distriution of bomb radiocarbon in the ocean. J. Geophys. Res., 90(C4), 6953–6970.

Broecker, W.S., S. Sutherland, and W. Smethie, 1995: Oceanic radiocarbon: separation of the natural and bomb components. Global Biogeochemical Cycles, 9(2), 263–288.

Duffy, P.B., P. Eltgroth, A. J. Bourgeois, and K. Caldeira, 1995: Effect of improved subgrid scale transport of tracers on uptake of bomb radiocarbon in the GFDL ocean general circulation model. Geophys. Res. Letters, 22(9), 1065–1068.

Ribbe, J., and M. Tomczak, 1995: Modelling radiocarbon uptake by the Southern Ocean. International WOCE Newsletter, 19, June 1995.

Ribbe, J., and M. Tomczak, 1996a: On the effect of the missing Indonesian throughflow in the Fine Resolution Antarctic Model (FRAM). J. Phys. Oceanogr. Submitted.

Ribbe, J., and M. Tomczak, 1996b: The formation of Subantarctic Mode Water in the Southeast Indian Ocean. J. Geophys. Res. Submitted.

Ribbe, J., and M. Tomczak, 1996c: On convection and subduction in the Fine Resolution Antarctic Model. J. Mar. Systems. Submitted.

Ribbe, J., J.T. Bye, G.E Jacobsen, E.M. Lawson, A.M. Smith, M. Tomczak, and Claudio Tuniz, 1996: First carbon-14 observations in waters of the Great Australian Bight. Nuclear Instruments and Methods in Physics Research, B52. Submitted.

Stuiver, M., and H.A Polach, 1977: Discussion: Reporting of C14 Data. Radiocarbon, 19(3), 355–363.

Vogel, J.C., and M. Marais, 1971: Pretoria radiocarbon Dates I. Radiocarbon, 13, 378–394.

WOCE Hydrographic Programme Office to Relocate

Following review of responses to the invitation for proposals to host the WHPO we have been informed by NSF that the office will be moving to the Scripps Institution of Oceanography under the direction of Drs James Swift and Lynne Talley. Financial support under the new contract will begin in FY 1997, probably in January, but possibly as early as November 1996. The proposal incorporates a strategy for a smooth transition from the present location in Woods Hole under the direction of Dr Terry Joyce.

On behalf of the SSG I would like to take this opportunity to thank Terry Joyce and all the staff who have worked with him, for their efforts to successfully establish the WHPO and to spin up what was to be the central data activity in WOCE. Jim Swift and Lynne Talley bring to the WHPO a wealth of experience since both have been PIs on numerous WOCE cruises. In addition Jim Swift is a former Chair of the WHP Planning Committee and Lynne Talley is co-Chair of the WOCE Synthesis and Modelling Working Group.

John Gould

Transport Estimates for the East Australian Current from the PCM3 Mooring Array

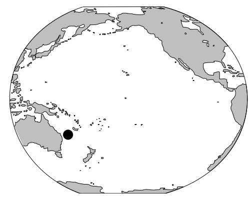

Matthias Tomczak and Peter Otto, Flinders Institute for Atmospheric and Marine Research, Flinders University, GPO Box 2100, Adelaide 5001; and John Church and Fred Boland, CSIRO Division of Oceanography, GPO Box 1538, Hobart, Tasmania 7001, Australia, M.Tomczak@es.flinders.edu.au

The Pacific mooring array PCM3 was located on the shelf and adjacent continental slope of Australia at approximately 30°S. It was designed to monitor the transport of the East Australian Current (EAC) for a period of at least two years while the WOCE Hydrographic Survey of the Pacific Ocean was in progress. This brief note summarises the first 10 months of observations.

Data and methods

The array was deployed in November 1991 by the Australian research vessel Franklin as a joint project between the CSIRO Division of Oceanography (the lead agency for the project) and the Flinders Institute for Atmospheric and Marine Research (FIAMS) of Flinders University. It was recovered during March 1994.

Data analysis was delayed by other commitments for everyone involved with the project, but in 1995 progress was made when Peter Otto agreed to choose the analysis of PCM3 data as the topic for his B.Sc. Honours thesis. Only the first 10 months of the observation period were processed at that time. This note therefore covers only the period November 1991 to September 1992. Hopefully, data analysis for the remainder of the data will proceed in the near future.

The array consisted of six moorings with Aanderaa current meters at the depths indicated in Fig. 1. Acoustic Doppler Current Profilers (ADCPs) were deployed at the top level of moorings #4 and #5, but the ADCP on mooring #5 malfunctioned and did not return data, and the ADCP on mooring #4 was only operational during the first 28 weeks.

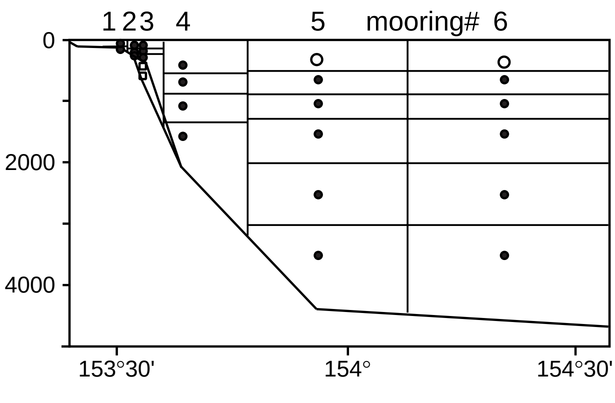

Figure 1. Sketch of WOCE mooring array PCM3. Dots: Aanderaa current meters, open circles: current meter underneath an ADCP (ADCPs were only operational during part of the period, and data from these instruments were not used in this analysis), open squares: current meters not included in this. Broken line: adjusted bottom topography, horizontal line: how the section was partitioned to calculate transports. Note that the top partitions extend the currents measured at the uppermost current meter into the surface, which in most situations underestimates the large surface current.

Ocean depth along the section was monitored by echo sounder when the array was deployed. As observed ocean depths were in reasonable agreement with information obtained from nautical charts and from a digital data base, a detailed topographic survey of the wider region was not obtained. From the observations it is now evident that mooring #3 was located in a canyon and that its lowest two current meters (the squares in Fig. 1) were sheltered from the effect of the EAC (Speeds at the two current meters are only 5–10% of the speeds observed both above and at the same level further offshore, and the direction is at the bottom current meter is onshore). In hindsight, the existence of a canyon in the region is not at variance with existing topographic information, but the location of the canyon cannot be determined with any certainty from the charts. To eliminate the effect of the canyon on our transport estimates we excluded the data from the lowest two instruments of mooring #3 from the analysis and assumed that the ocean floor has the shape indicated by the dotted line in Fig. 1. The data from all other instruments were low-passed and decimated to hourly values. Progressive vector diagrams were used to verify that the predominant current direction was perpendicular to the mean orientation of the mooring array (115°), and the records were resolved into components perpendicular and parallel to 115° true. These components were then compressed into weekly averages.

Transport estimates were derived by dividing the cross sectional area along the mooring array into rectangles centred on the instruments (Fig. 1) and assuming that currents were uniform over each rectangle.

Results and discussion

Fig. 2 shows the total volume transport across the mooring array calculated from the weekly data. The outstanding feature are the persistent current reversals during the summer of 1991/92 (November–March).

The high level of variability in the EAC is well known, but it is usually believed to be associated with eddies. However, when the transport is analysed for individual moorings (*i.e.* calculated for cross-sections defined by halfway points between moorings as indicated in Fig. 1) it is seen that the observed current reversals propagate through the array from east to west and cannot easily be attributed to eddies. Visual inspection of transport time series (Fig. 3) suggests a phase lag between moorings

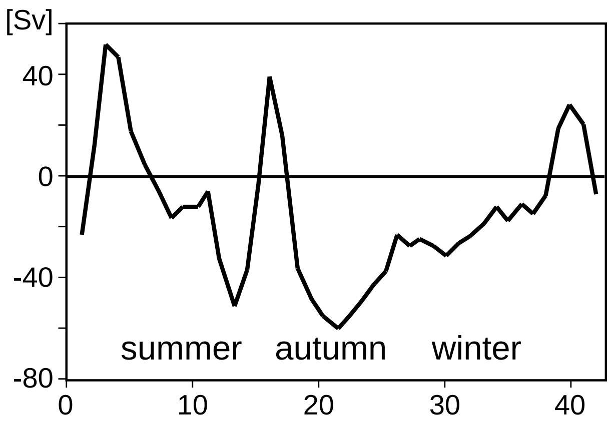

Figure 2. Total volume transport (Sv) of the East Australian Current across mooring array PCM3.

#4 and #6 of about 3.5 weeks and a phase lag between moorings #2 and #6 of about 5 weeks. The observed phase lags (which were determined quantitatively by cross-correlation analysis) give an average westward propagation speed of just under 0.03 m/s. This compares with the propagation speed of baroclinic Rossby waves, using Tasman Sea summer conditions, of 0.033 m/s. We therefore suggest that the observed current reversals are associated with baroclinic Rossby waves and not necessarily with eddies.

Whether current reversals of the EAC near 30°S are a regular summer phenomenon or a particular feature of the 1991/92 summer period cannot be said with any certainty until we see the results from the entire time series. The analysis of Godfrey (1973) and Hamon *et al.* (1975) clearly demonstrates that the EAC is generally stronger during summer than during winter and reverses only rarely. Based on the data from PCM3 the EAC seemed to be weaker on average during the 1991/92 summer than during the following winter, which seems to be at variance with Godfrey's (1973) climatological mean situation.

The data presented by Hamon *et al*. (1975) compare somewhat more favourably with our observations. They show large quasi-periodic fluctuations of current speed during the summer months with the same periodicity of about 10 weeks seen in our data but no current reversals over the deep ocean (current reversals do occur on the shelf in their data). The fluctuations move southward with a propagation speed of about 0.4 m/s. This has commonly been interpreted as reflecting the southward movement of eddies.

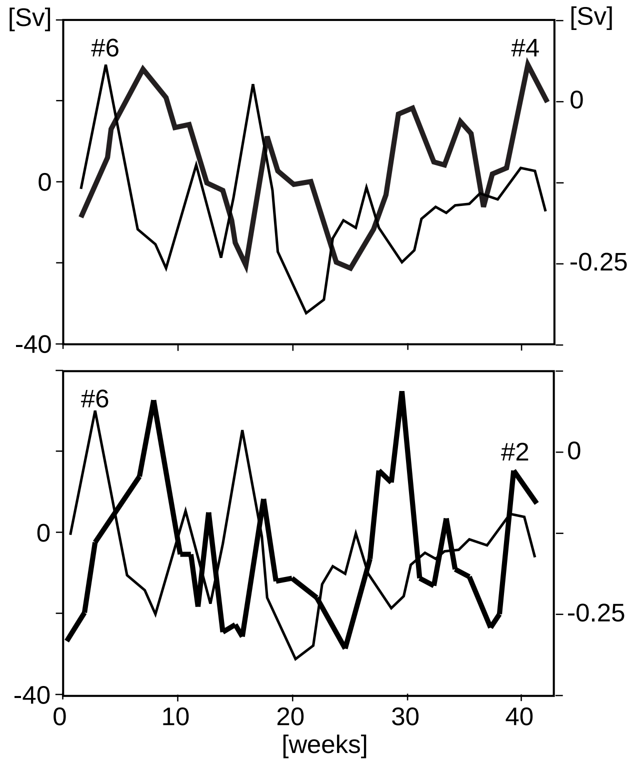

Figure 3. Comparison of volume transports (Sv) across parts of the EAC defined by areas around individual moorings. (a) mooring #4 (heavy line and right hand scale) against mooring #6 (thin line and left hand scale); (b) mooring #2 (heavy line and right hand scale) against mooring #6 (thin line and left hand scale).

The analysis of Godfrey (1973) and Hamon *et al.* (1975) is based on ship drift data and does not include subsurface transports. The combination of our current meter data with CTD information from WOCE repeat sections across PCM3 can throw light on the question how representative the current meter data are for the EAC at the surface; this task remains to be done.

References

Godfrey, J.S., 1973: Comparison of the East Australian Current with the western boundary flow in Bryan and Cox's (1968) numerical model ocean. Deep-Sea Res., 20, 1059–1076.

Hamon, B.V., J.S. Godfrey and M.A. Greig, 1975: Relation between mean sea level, current and wind stress on the east coast of Australia. Australian J. Mar. and Freshwater Res., 26, 389–403.

WOCE Current Meter Statistics Available NOW

In the April issue of the Newsletter we reported the posting on the IPO homepage of current meter statistics from pre-WOCE deployments. Now we are delighted to report that at the Oregon State University (OSU) Current Meter DAC statistics from WOCE records are available now!

For each of the ten WOCE data sets presently at OSU a table of statistics can be accessed. Each table contains the location, duration, depth and means, and variances and co-variances of the quantities measured. Amongst other uses these two data sets should allow modellers to access the realism of their OGCMs. Both data sets can be reached from either:

http://tethys.oce.orst.edu/form15.html

or

http://www.soc.soton.ac.uk/OTHERS/woceipo/data.html

MICOM-based Global Modelling in the US

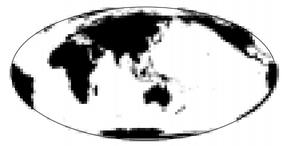

Rainer Bleck, Rosenstiel School of Marine and Atmospheric Science, University of Miami, Miami, FL 33149, USA, bleck@nutmeg.rsmas.miami.edu

This article describes the current status of climate-oriented global ocean modelling carried out by researchers at the University of Miami with a locally developed circulation model.

Together with the OPYC model developed by J. Oberhuber at the Max Planck Institute for Meteorology in Hamburg, the Miami Isopycnic Coordinate Ocean Model (MICOM) is one of two "general-purpose" isopycnic models available to the community today. Unlike OPYC, MICOM presently lacks a sea ice component, but it has numerical attributes that allow it to run fairly efficiently at high resolution on massively parallel processors (MPPs). A recently completed 2-year, 1/12-degree simulation of the North and Equatorial Atlantic, which yielded Gulf Stream details not previously seen in basin-scale simulations, is one example of what can be achieved with isopycnic models run on modern supercomputers. (Results from this experiment are on display at the Web site http://everest.ee.umn.edu/~sawdey/micom.html.)

The 1/12 degree Atlantic simulation just mentioned was obtained with a message-passing version of MICOM, in which communication between individual processors – each of which "owns" a piece of the overall model domain – is the responsibility of the programmer. An alternate way of writing programs for MPPs is to make use of data-parallel programming languages such as Fortran-90. Here, arithmetic operations referencing individual grid points are replaced by matrix operations that apply to the grid as a whole. Data-parallel languages don't do away with inter-processor communication, but they hide the message passing chores from the applications programmer.

Collaboration of the Miami ocean modellers with computer scientists looking for application codes suitable for MPPs has led to the creation of both message-passing and data-parallel versions of MICOM. The data-parallel version was written at the Los Alamos National Laboratory for the purpose of testing the model on the Connection Machine (CM-5) as a possible component in a climate model under development there.

As a 3-dimensional primitive-equation model, MICOM is too slow to be integrated for thousands of years, especially if configured with a mesh size of 20– 30 km that (marginally) resolves barotropic and baroclinic instability processes. However, century-long global integrations with this mesh size are feasible on today's MPPs.

Two near-global, intermediate-resolution experiments (1.4° horizontal mesh size) are currently underway in Los Alamos to assess the effect of diapycnal mixing on the thermohaline circulation. Isopycnic coordinate models are ideally suited for this type of sensitivity study, since they are not burdened by numerically induced background vertical mixing. The work is primarily supported by the US Department of Energy.

In the present runs we use 16 layers and 128 x 256 square grid cells on a Mercator map spanning the latitude range 68°S–63°N. The circulation is driven by seasonally varying fields of wind stress, atmospheric temperature and humidity derived from the COADS data set, precipitation inferred from the NOAA microwave sounder, net radiation from the Oberhuber atlas, and freshwater input from 14 major rivers and the polar ice caps. No information about conditions outside the model domain is supplied at the northern and southern domain boundaries. Note that we are forcing the model with atmospheric data, as opposed to oceanic (sea surface) data.

Earlier global experiments comparing the performance of the 1.4° model with a 0.35° fine-mesh version ran to years 425 and 52, respectively, but were discontinued due to concern over a subtle inconsistency between the standard and the data-parallel model version. The present round of experiments is confined to non-eddy-resolving grid resolution, but a 0.225° simulation will be initiated as soon as fields from a 100-year 1.4° start-up run are available.

Emphasis in our present analysis of model output is on the global overturning circulation – the conveyor belt – and on details of interlayer or diapycnal mass exchange. The latter is driven in the model by two processes: the annual mixed-layer advance/retreat and interior diapycnal mixing.

At this stage, we are not discovering anything new but are trying to confirm that the model is functioning properly. Among the phenomena that come to light are the following:

1. The three major ocean basins are known to contribute quite differently to the global thermohaline circulation. The model's way of depicting these differences is shown in Fig. 1. In the Atlantic (upper left panel) we see an interhemispheric overturning cell which after 75 yrs of integration remains at a steady 21 Sv. The maximum northward heat flux associated with this cell is 0.85 PW. Given the absence of the Arctic basin from the model, the overturning rate is surprisingly high. One possible contributing factor is our method of basing evaporation on prescribed atmospheric humidity; this causes water that is slightly too warm relative to climatology to become too salty as well. The resulting buoyancy loss creates a positive feedback on the maintenance of the overturning cell.
2. The counterclockwise circulation around Australia (~15 Sv – slightly on the high side) has been removed from the streamfunction plots for the Indian and

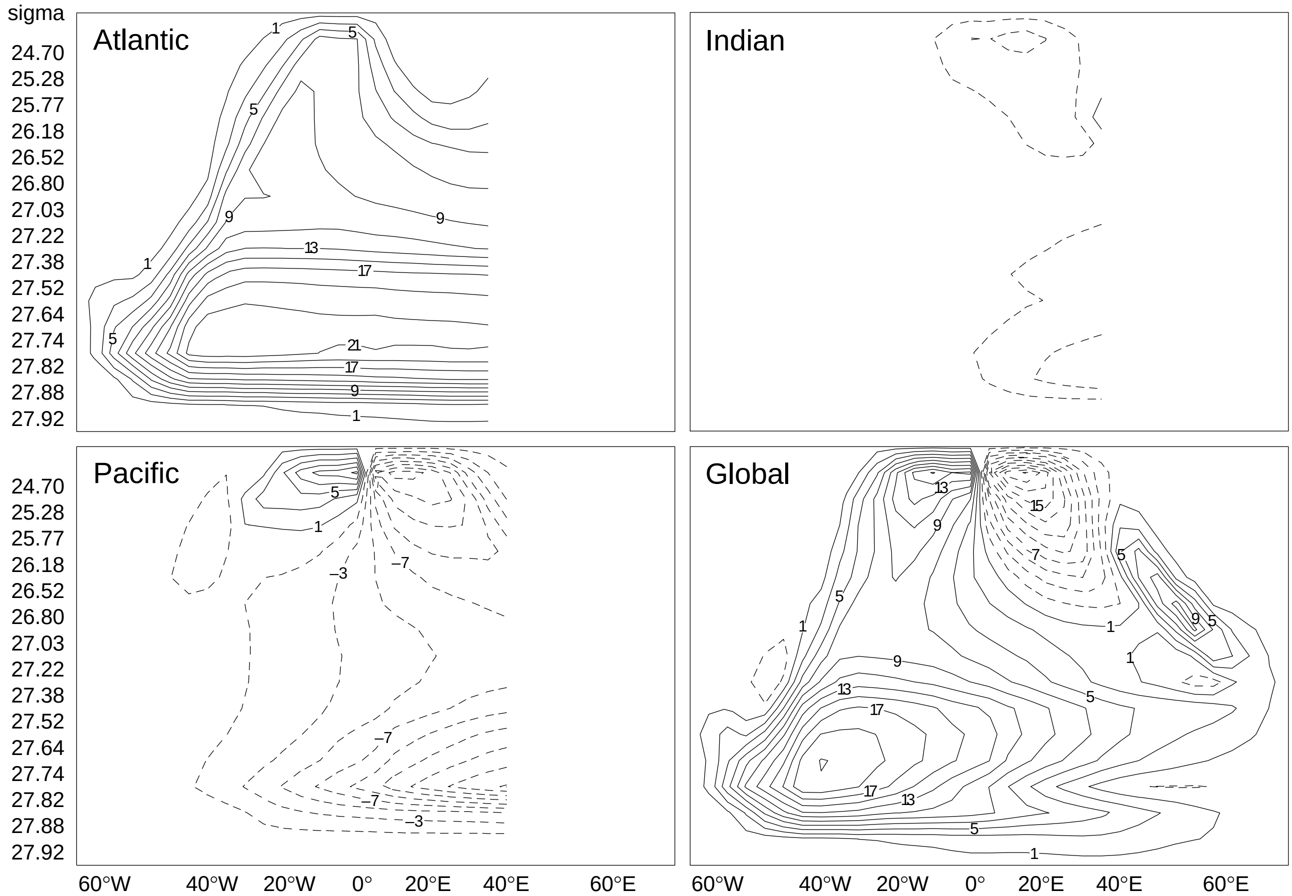

Figure 1. 5-year averaged mass transport in the vertical-meridional plane, zonally averaged over 3 individual ocean basins and the world ocean as a whole. Solid/dashed lines indicate counterclockwise/clockwise rotation looking east. Contour interval: 2 Sv.

Pacific Oceans (upper right and lower left panels of Fig. 1) to eliminate the discontinuity that otherwise would appear at the latitude of the Indonesian throughflow. The residual circulation shows 4–5 Sv abyssal upwelling in the abyssal Indian Ocean (a rather low value) while the equatorial Pacific appears as the place where wind-driven divergence pulls most of the global conveyor belt water back to the surface.

3. The zonally averaged overturning circulation in all basins combined is shown in the lower right panel of Fig. 1. A noteworthy feature is the thermally indirect Deacon cell in the southern ocean. The meridional heat flux at this time reaches values of +1.2 PW at 18°N and -1.0 Sv at 22°S. Note that the model produces no Antarctic Bottom Water. AABW formation is presently inhibited by our crude method of distributing melt water uniformly in longitude and time along the northern and southern model boundaries.

4. More detailed geographic information about the thermohaline circulation can be gleaned from maps of interlayer mass transport. To give an example, we show in Fig. 2 (page 22) the annually averaged vertical mass flux through the bottom of the mixed layer. The largest transport values are found in the Labrador Sea where the Labrador Current impinging on a sloping wintertime mixed-layer interface subducts ~1500 m of water every year, and in the east-central Pacific where water is pulled up into the mixed layer at a rate of almost 1000 m per year. Fig. 2 suggests that the subduction scenario just outlined for the Labrador Current holds in general: if averaged over an annual cycle, water flowing equatorward tends to be subducted while water flowing poleward tends to enter the mixed layer.

While diagnosis of the subduction process in Cartesian coordinates involves evaluating the strength of the meridional flow in relation to the meridional slope of the mixed-layer interface, the mechanics of MICOM's variable-depth slab-type mixed layer allows this transport to be diagnosed very simply as a *vertical* mass exchange. In a nutshell, an equatorward flowing current will tend to push the mixed-layer interface equatorward. From an Eulerian perspective, this is seen as mixed-layer deepening, and the local surface buoyancy fluxes will try to restore the "correct" mixed-layer depth. The amount of water thereby transferred from the mixed layer to the layer(s) below matches the amount that earlier would have crossed the interface horizontally, had the interface not been carried along with the motion. An analogous argument can be made for poleward motion.

Many features in the MICOM solutions appear realistic, but various simplifications made in setting up this experiment are coming back to haunt us. The fact that the model appears to be "comfortable" with forcing fields based on the presently observed atmosphere, at least on a 100-yr time scale, is perhaps the most noteworthy result. The reader should be reminded that isopycnal modelling work is partly driven by the community's need for models that are able to reproduce the present ocean-atmosphere climate without the help of "flux corrections" – artificial heat sources and sinks introduced to compensate for model biases. So far, the investment seems to be paying off.

BIO Hesperides Covered WOCE SR1b in February 1995

Marc A. Garcia, Universitat Politecnica de Catalunya, Barcelona, Spain, mgarcial@etseccpb.upc.es

In the framework of the Spanish contribution to WOCE, BIO Hesperides covered the WOCE SR1b section across the Drake Passage in February 1995. 21 hydrographic stations with 20 nm characteristic spacing were occupied along the Burdwood Bank–Elephant Island transect 15–20 February 1995. At each station, surface-to-bottom CTD casts were performed with a GO MkIIIC CTD probe equipped with temperature, salinity, dissolved oxygen, fluorescence and light transmission sensors. Water samples were obtained at 24 levels on each station. Some of the bottles carried SIS RTM 4002 reversible digital thermometers. At the southernmost part of the section, a number of expendable XCTD probes were launched between adjacent CTD stations with the aim of identifying small-scale hydrographic structures at the Antarctic Zone. Throughout the cruise, routine continuous measurements of surface T and S were made by means of a SBE 21 thermosalinograph. Both *en-route* and on-station ADCP velocity profiles were obtained through a hull-mounted RDI 150 kHz NarrowBand system. The Skyfix station located in the Falkland Islands was used for DGPS positioning. All water samples were analyzed on board during the cruise. The properties calculated from water samples were salinity, dissolved oxygen concentration, nutrients and Chlorophyll. All analyses were carried out according to the corresponding WHP specifications. Fractions of the water samples corresponding to the uppermost layers were preserved for post-cruise phytoplankton taxonomy studies.

Fronts, water masses and circulation across SR1b in February 1995

Figs. 1 and 2 show the vertical distributions of potential temperature and salinity on WOCE SR1b section as derived from the DRAKE 95 preliminary dataset. The q and S fields have been interpolated using a spatial objective analysis technique. The three fronts which define the classical zonation of the ACC can be easily traced in the distributions of physical parameters. At the time of the cruise, the Subantarctic Front (SAF) was located at 55°55'S, the Polar Front (PF) at 57°20'S and the Continental Water Boundary (CWB) at 60°45'S, *i.e.* on the northern continental slope of the South Shetland Islands.

The location of the SAF can be deduced from the steepness of the 3°C to 5°C isotherms, which is known to be maximum at this ACC front (Fig. 1). North of the SAF, there is a rapid deepening of the subsurface salinity minimum which characterizes the Antarctic Intermediate Water (AAIW). During the DRAKE 95 cruise, we observed the presence of AAIW at 56°S at depths of the order of 200 m; at 55°S, the AAIW salinity minimum was at 600 m depth. According to Peterson and Whitworth (1989), we consider that the "core" of the SAF was located at the latitude where the 4°C isotherm intersected the 200 m layer. On the other hand, the PF is, from the hydrographic point of view, the northern boundary of the Antarctic Surface Water (AASW), which is characterized by a subsurface temperature minimum embedded in an intense halocline (Peterson and Stramma, 1991). According to the criteria proposed by Deacon (1933) and Peterson and Whitworth (1989), we assume that the PF was located where the temperature minimum sinked below the 200 m depth. The CWB is the

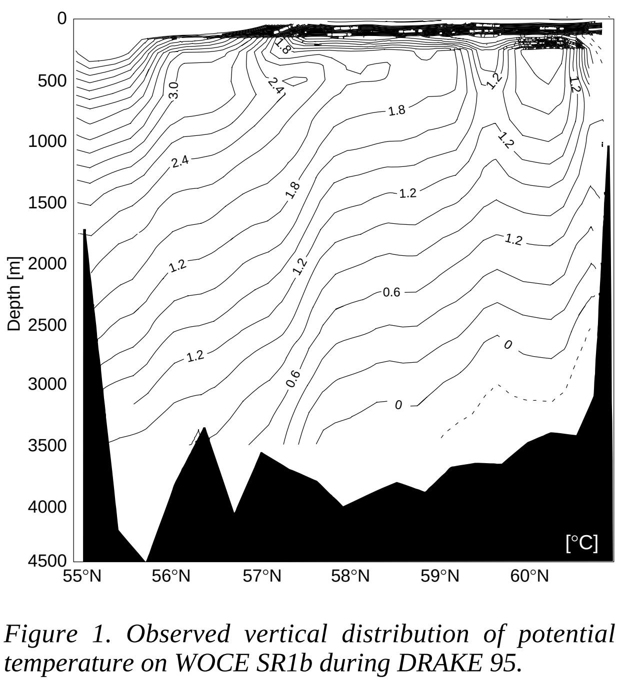

Figure 1. Observed vertical distribution of potential temperature on WOCE SR1b during DRAKE 95.

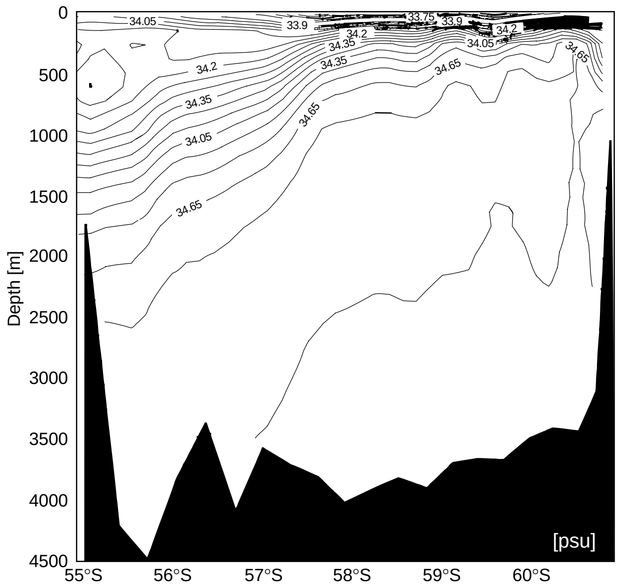

Figure 2. Observed vertical distribution of salinity on WOCE SR1b during DRAKE 95.

northernmost extent of a cool and relatively uniform water mass produced in the Weddell Sea which spreads onto the northern continental slope of the South Shetland Islands at depths between 150 m and 500 m (Deacon, 1933; Sievers and Emery, 1978). The CWB can be envisaged as the western extension of the Scotia Front (Gordon, 1967; Smith, 1989). We consider that the CWB was located at the depth where the 0°C isotherm intersected the 300 m depth layer.

The hydrographic characteristics of the water masses lying above the AAIW north of the SAF are those typical of the Subantarctic Surface Water. The Upper and Lower Circumpolar Deep Water layers (UCDW and LCDW) underlie the waters of Antarctic origin, *i.e.* AASW and AAIW. The salinity maximum is contained into the LCDW layer (Fig. 2), whereas the deep temperature maximum is the signature of the UCDW south of the SAF. The ascent of the LCDW layer is impressive: the salinity maximum was at a 3500 m depth at 56°S, and only at 1500 m at 60°S. The signature of the UCDW was lost north of the CWB. Below the LCDW layer we observed negative potential temperatures which are characteristic of the Weddell Sea Deep Water outflow. Fig. 3 suggests that WSDW was flowing westward across SR1b.

Our preliminary ADCP results (not shown here) show a multi-jet structure of the ACC which is in agreement with the description made by other authors. Maximum velocities to the NE of the order of 50 cm/s were attained at the surface mixed layer within the current bands related to the SAF and PF. Bands of westward flow were observed south of the PF.

Fig. 3 shows the vertical distribution of the geostrophic velocity across SR1b computed with a 3500 dbar reference level. The profiles corresponding to shallower depths have been "filled up" by means of an extrapolation method based on principal component analysis. Pairs of baroclinic jets associated to the SAF and the PF can be easily identified. At the SAF band, maximum surface geostrophic velocities of 50 cm/s are reached, which is in agreement with the ADCP measurements. The flow associated to the PF is slightly slower than the SAF jets. The eastward flow is weakest in the Antarctic Zone, *i.e.* between the PF and the CWB. The eastward jet centred on 59°S is probably the kinematic expression of the Southern ACC Front discussed by Orsi (1993) and Read *et al.* (1995). As for the westward flow band centred on 59°55'S, we believe that this structure is linked to current meandering related to the bottom topography, rather than to an eddy. During the DRAKE 95 cruise, the net geostrophic transport of the ACC across WOCE SR1b was 145 Sv (relative to 3500 dbar).

Acknowledgements

The work described above was carried out by: Oswaldo Lopez, M. Pilar Rojas, Joaquim Sospedra, Damia Gomis, Antonio Cruzado, Zoila Velasquez, Albert Palanques, Pere Puig, Mario Manriquez, Pedro Jornet, Pablo Rodriguez, Jose Escanez and Antoni Calafat.

We acknowledge the expert support of the crew of BIO Hesperides during the DRAKE 95 cruise. We are specially thankful to Guillermo Sanchez and Manuel Velarde for their repair of the Rosette lower plate, which enabled us to obtain water samples at 24 levels throughout the cruise. We also thank Robert Kluckholm and the team of Antarctic Support Associates at Punta Arenas for their help. The authors are equally grateful to Robert Millard Jr., who provided guidance for the CTD data postprocessing work. DRAKE 95 was funded by the Spanish Comision Interministerial de Ciencia y Tecnologia, grants Nos. AMB94-0436 and AMB94-1523-E.

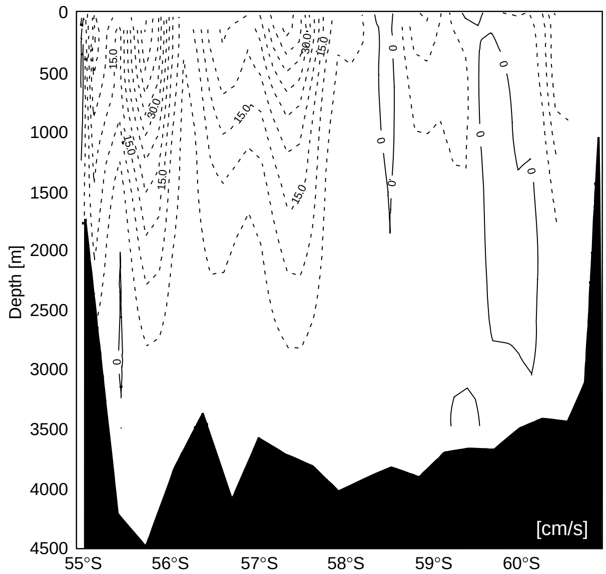

Figure 3. Computed geostrophic velocities across WOCE SR1b during DRAKE 95 with respect to a 3500 dbar reference level. Dashed lines mean eastward velocities, solid lines mean westward velocities.

References

Deacon, G.E.R., 1933: A general account of the hydrology of the South Atlantic Ocean. Discovery Reports, 7, 171–238.

Gordon, A.L., 1967: Geostrophic transport through the Drake Passage. Science, 156, 1732–1734.

Orsi, A.H., 1993: On the extent of frontal structure of the Antarctic Circumpolar Current. PhD Thesis, Texas A&M University, TX, USA, 74pp.

Peterson, R.G., and L. Stramma, L. 1991: Upper-level circulation in the South Atlantic Ocean. Progr. Oceanogr., 26, 1–73.

Peterson, R.G., and T. Whitworth III, 1989: The Subantarctic and Polar fronts in relation to deep water masses through the Southwestern Atlantic. J. Geophys. Res., 94, 10817–10838.

Read, J.F., R.T. Pollard, A.I. Morrison, and C. Symon, 1995: On the southerly extent of the Antarctic Circumpolar Current in the southeast Pacific. Deep-Sea Res., part II, 42, 933–954.

Sievers, H.A., and W.J. Emery, 1978: Variability of the Antarctic Polar Frontal Zone in Drake Passage - summer 1976–1977. J. Geophys. Res., 83, 3010–3022.

Smith, S.G., 1989: On the Weddell–Scotia Confluence and the Scotia Front. MSc Thesis, Texas A&M University, TX, USA, 85pp.

Water Mass Analysis as a Tool for Climate Research

A workshop to be held during the 1997 IAMAS/IAPSO Joint Assembly (Melbourne, Australia, 1–9 July 1997)

The ocean is the flywheel of the climate machine. Its effect on the operation of this machine requires accurate estimates of turnover rates and associated heat and freshwater fluxes. The traditional oceanographic approach to study this process is to trace the distribution of water properties, in a procedure usually labelled Water Mass Analysis. The technique continues to be an effective tool in building an understanding of the patterns of ocean circulation and mixing and as such is an important component of international programmes such as WOCE and CLIVAR.

Modern water mass analysis can make use of analytical and modelling methods that were not available to oceanographers when water mass analysis was first introduced. In addition, it has available a wider suite of chemical tracers to describe water masses. Questions such as isopycnal vs. diapycnal mixing, mixing between and within water masses, and age determination in a mixture of water masses of different age can now all be tackled quantitatively.

A workshop to evaluate the status of water mass research and its links with climate studies and ocean modelling will be held during the 1997 IAMAS/IAPSO Joint Assembly. It aims to bring together physical oceanographers, tracer oceanographers and numerical modellers in a discussion of modern quantitative methods of water mass analysis and their use in climate research. If you are interested in the workshop, notify the convenor or one of the co-convenors of your intention to participate. A working document will be sent out to you in May 1997 if you notify us before then.

Convenor:

Matthias Tomczak
FIAMS, Flinders University of South Australia
GPO Box 2100, Adelaide, S.A. 5001, Australia
phone +61-8-201-2298
fax +61-8-201-3573
e-mail matthias.tomczak@flinders.edu.au.

Co-convenors:

Arnold L. Gordon
Lamont-Doherty Earth Observatory
Palisades, NY 10964-8000, USA
phone +1-914-365 8325
fax +1-914-365-8157
e-mail agordon@ldeo.columbia.edu.

Lynne Talley
Scripps Institution of Oceanography 0230
UCSD, 9500 Gilman Dr.
La Jolla, CA 92093-0230, USA
phone +1-619-534-6610
fax +1-619-534-9696
e-mail ltalley@ucsd.edu.

Preliminary Announcement of the WOCE Southern Ocean Workshop

This will be held at the Antarctic Cooperative Research Centre (CRC), University of Tasmania, Hobart, Australia, 8–12 July 1997. The local organiser will be Steve Rintoul (CSIRO, Hobart). He is assisted by a scientific organising committee consisting of

Nathan Bindoff (Antarctic CRC, Hobart)
Dudley Chelton (Oregon State University, USA)
Eberhard Fahrbach (AWI, Bremerhaven, Germany)
Brian King (SOC, Southampton, UK)
Eric Lindstrom (US-GOOS Office, Washington, DC, USA)
Kevin Speer (LPO/UM Ifremer, Brest, France)
Mark Warner (U. Washington, Seattle, USA)
David Webb (SOC, Southampton, UK).

The Workshop is sandwiched between the IAMAP/IAPSO meeting in Melbourne, Australia (1–9 July) and a conference on “Antarctica and Global Change” to be held at the Antarctic CRC, 13–18 July.

It is planned that the juxtaposition of these three meetings will help to minimise travel and to encourage participation.

A further announcement seeking initial expressions of interest in attending the WOCE workshop will appear in the next WOCE Newsletter.

Upper Ocean Thermal Data and Products

N.P. Holliday, WOCE IPO, Southampton Oceanography Centre, Empress Dock, Southampton, SO14 3ZH, UK, penny.holliday@soc.soton.ac.uk

The WOCE Upper Ocean Thermal Data Assembly Centres (UOT DACs) have two objectives: to generate a consistent high quality global data set of upper ocean temperature profiles, and to construct products from the quality controlled data. The UOT DAC is a cooperative venture between national data centres in USA, France, Australia and Canada working with science centres in USA (SIO and AOML) and Australia (CSIRO), and is part of the IOC-WMO's Global Temperature and Salinity Pilot Project (GTSPP). In the last issue of this Newsletter (Number 22, April 1996), the Pacific Science Centre (Joint Environmental Data Analysis Centre, SIO) and the Global Subsurface Data Centre (GSDC, IFREMER, France) described their activities and products.

Upper ocean thermal data is predominantly generated by Expendable Bathythermographs (XBTs) but the GTSPP data set also contains data from CTDs, moored buoys, thermistor chains on surface drifters, and profiling floats. There are two main categories of data; low resolution inflexion point data usually received in "real-time" (30 days after collection), and high resolution data received in "delayed mode", several months to several years after collection. Because of the delayed submission, the 1990 data set has a higher number of high resolution data than recent years. Obtaining the delayed mode data in a timely way (within a year of collection) is a priority for WOCE.

The UOT DAC has two levels of quality control: the GTSPP procedures, which essentially are consistency checks (date, time, position, speed and comparison to climatology), and the scientific quality control. The latter utilises the knowledge of the science centres to distinguish between instrument failures and real features in the data, and to assign a quality flag to each data point. During scientific quality control, all profiles are passed through a series of tests and individually inspected. Mapping of temperature and heat storage anomalies, and comparison with neighbouring profiles in time and space are also employed to detect problem data. The science centres quality control the "best set" of data on a yearly basis, *i.e.*, all the high resolution profiles and any inflexion point profiles for which the equivalent high resolution data have not been received.

WOCE UOT DAC science centres are not permanent quality control centres, and it is envisaged that their roles will eventually be fulfilled by national data centres. At the recent joint meeting of the GTSPP Steering Committee and the WOCE UOT DAC (April 1996) it was agreed to develop a formal mechanism for transferring the techniques and expertise of the science centres to the national data centres over the coming years. This process will take considerable time and resources to be implemented, but it is considered essential for the success of future long-term climate study programmes.

Upper Ocean Thermal Data and Product Availability

- **GTSPP Quality Controlled Temperature Profiles (NODC)**

http://www.nodc.noaa.gov/GTSPP/gtspp-home.html

Inflexion point data	1990–1996	Over 300,000 profiles
High resolution data	1990–1996	Over 130,000 profiles

- **Scientific Quality Controlled Temperature Profiles: "Best Set" (NODC)**

http://www.nodc.noaa.gov/GTSPP/gtspp-home.html

Pacific Ocean	1990–1992
Indian Ocean	1990–1991
Atlantic Ocean	1990–1991

- **Products from National Data Centres (NODC, MEDS, IFREMER)**

http://www.meds.dfo.ca/MEDS/e_home.html
http://www.ifremer.fr/sismer/program/gsdc/homepage.html
Quarterly reports of number of observations along WOCE lines
Monthly reports of vessels with data reporting problems
Monthly reports of real-time data flow failures
Data set statistics and data distribution maps

- **Products from the Pacific Science Centre (JEDA Centre, SIO)**

http://cyberia.ucsd.edu/jeda.html
Data distribution maps
Temperature climatology
Real-time analysis; bimonthly maps of sea surface temperature and heat storage anomalies
Animations of mapping exercises
Historical analyses; gridded fields used in creating temperature anomalies
Images of ocean temperature anomalies; heat storage and surface temperature

- **Products soon to be available from the Atlantic Science Centre (AOML) and Indian Ocean Science Centre (CSIRO)**

http://www.aoml.noaa.gov/phod/uot/
Data distribution maps
Temperature climatology
Maps of ocean temperature anomalies, heat storage and surface temperatures.

New Handbook of Quality Control Procedures and Methods for Surface Meteorology Data Available Now!

The WOCE Data Assembly Center (DAC) for Surface Meteorology at the Florida State University is charged with collecting, quality controlling, archiving and distributing all underway surface meteorology data from WOCE vessels worldwide. Types of data collected include standard ship bridge observations, advanced automated systems and all other practically obtainable surface meteorological data from WOCE research vessels and buoys.

The focus of the handbook is to describe the methodology and detail the quality control procedures. The DAC intends for this document to be used by the WOCE scientific community as well as other interested researchers.

After all evaluation of a data set is complete, a final network Common Data Format (netCDF) file is created. The data are also converted to standard ASCII format, and all QC reports are made available in a text format. All reports, netCDF, and ASCII data are available along with cruise track plots and data availabilty lists.

The primary method to access the data will be via the world wide web. The address of the WOCE DAC homepage is:

http://www.coaps.fsu.edu/WOCE

The data are also available via anonymous ftp from:

wocemet.fsu.edu

The data are located in the **'/pub/WOCE/'** directory.

The handbook (WOCE Report No. 141/96) can be ordered directly from:

WOCE DAC/SAC
Center for Ocean and Atmospheric Prediction Studies
Florida State University
2035 E. Dirac Drive/Suite 200 Johnson Bldg.
Tallahassee, FL 32310
USA.

Meeting Timetable 1996

WOCE Meetings

August 27–30	US WOCE SSC	Arlington,VA
October 7–9	WHP-15	Woods Hole, MA
October 15–17	WOCE-23	Southampton

Science and Other Meetings

July 23–27	AGU Western Pacific Geophysics Meeting, Brisbane
August 12–16	Pacific Ocean Remote Sensing Conference, Victoria, BC
August 19–23	WOCE Pacific Workshop, Newport Beach, CA
September 4–6	CLIVAR DecCen Workshop on the Induction of DecCen Climate Variability by Large Scale Atmosphere-Ocean Interactions, Vancouver, BC
September 9–11	CLIVAR NEG-2, 2nd session, Victoria, BC
September 27–October 1	ICES Annual Science Conference, Special WOCE/JGOFS/CLIVAR Session, Reyjkavik
October 7–11	First International Conference on EuroGOOS, Den Haag
October 21–25	CLIVAR Upper Ocean Observations Workshop and CLIVAR Upper Ocean Panel, 2nd session, Villefranche-sur-Mer
October 28–31	CLIVAR DecCen Ocean Circulation and Climate Workshop, Villefranche-sur-Mer
November 18–23	The North Atlantic: Ocean Currents, Climate, Weather and Environment, Copenhagen

For more information on the above meetings contact the IPO. If you are aware of any conferences or workshops which are suitable for the presentation of WOCE results and are not mentioned in the above list please let the IPO know.

WOCE's legacy to CLIVAR

W. John Gould, WOCE IPO

At the CLIVAR SSG in Sapporo John Church and John Gould presented papers based on

(a) what observations initiated or maintained under WOCE might be considered for incorporation in a CLIVAR Implementation Plan and

(b) the structure and function of the WOCE data system so that the CLIVAR SSG could consider how elements of it might serve CLIVAR needs.

There has been discussion of these documents since the Sapporo meeting and revised versions are to be tabled at the Villefranche CLIVAR DecCen workshop in November 1996. In the meantime we felt we should summarise these papers in the WOCE and CLIVAR Newsletters.

Although assessment of decadal variability in the ocean has in some senses been a secondary objective of WOCE, much has been learned by WOCE and much more might be learned by providing continuity between the WOCE 1990-1997 observational phase and the 15 year CLIVAR programme.

Issues highlighted in the observational paper were:

- Meridional heat fluxes have been or will be computed on a number of trans-basin WOCE sections but little if anything is known from observations about seasonal and interannual changes in these fluxes. It was suggested therefore that CLIVAR observational strategy for flux determinations should
  - focus on zonal sections used in WOCE.
  - repeat these at intervals chosen by CLIVAR to determine seasonal, interannual and longer-period changes in oceanic fluxes.
  - build on the experience gained during WOCE to optimise observational techniques.
- There are seasonal and interannual changes in the properties and distributions of winter-modified water masses and in the strengths and positions of inter-gyre boundaries. Meridional sections can document these changes. During WOCE, such sections were supplemented by intensive surveys of upper ocean properties (*e.g.* the N. Atlantic Vivaldi surveys of 1991 and 1996). CLIVAR might consider incorporating observations that would build on these WOCE measurements.
- Repeated sections across major current systems and inter-basin channels have been made in WOCE and should be considered for continuation by CLIVAR in order to document changes in circulation. Western boundary currents are major elements of the global circulation and are important in determining meridional fluxes. Where direct measurements of these currents exist they should continue.
- Some time-series stations and sections started many years earlier, were assimilated into WOCE plans. Many more were recommended by WOCE but were not implemented due to shortage of resources. The recent development of moored profiling CTD systems might permit many new time-series stations. However they would not allow the comprehensive additional observations that add value to, for instance, the BATS and HOTS time series.
- TOGA and WOCE developed a global network of high density (eddy resolving) and low density XBT lines to identify upper ocean thermal anomalies and to allow measurements of heat storage. It is envisaged that the low density XBT network will be incorporated in GOOS. High density lines need to continue as a research activity under CLIVAR. Routine measurements of surface salinity from the VOS fleet would provide a means of observing the development and propagation of surface salinity anomalies. The programme of instrumenting the VOS fleet with salinity sensors should therefore continue and be expanded under CLIVAR. Near-global coverage would require salinity sensors on floats and drifters.
- The observational strategy for deployment of surface drifters of the TOGA/WOCE design is a matter for discussion in the CLIVAR Upper Ocean Panel.
- The widespread deployment of ALACE floats has been a major element of WOCE. The profiling PALACE is a powerful new tool with which to explore and monitor upper 1500 m temperature and salinity particularly in remote areas. CLIVAR should consider therefore the deployment of PALACE floats in considerable numbers. The dominance of mesoscale variability requires large numbers of floats to produce the stable mean flow statistics needed to assess low-frequency variability. Thus the manner in which floats might be used to assess ocean circulation variability needs further consideration.
- Satellite altimetry has shed light on variability in the open ocean and CLIVAR and WOCE have jointly pressed for the continuation of TOPEX/POSEIDON-quality altimetric missions. The requirement for *in-situ* coastal sea level measurements however remains as a means of providing continuous long time series of guaranteed quality and as a reference for altimeter missions. Of particular importance should be sea level measurements across choke points.

The figure at the bottom of page 22 shows a possible configuration for elements of WOCE-based CLIVAR observations.

In respect of the WOCE data system, the CLIVAR SSG recognised the advantages of building on a system already developed within WCRP but stressed that CLIVAR would place a stronger emphasis on the delivery of real-time data than was the case in WOCE. This is clearly an important area of change and a small ad-hoc WOCE/CLIVAR group will be asked to consider the appropriateness of the WOCE data system for CLIVAR's needs.

First Announcement of the WOCE South Atlantic Workshop

The World Ocean Circulation Experiment announces a workshop on the large scale circulation and dynamics of the Southern and Equatorial Atlantic Ocean, to be held in Brest (France), 16–20 June 1997. The goals of the workshop are to summarize scientific results obtained so far, to identify significant outstanding problems where progress has to be made to reach the goals of WOCE, to encourage and facilitate collaboration among the scientists involved, and to prepare data synthesis and joint publications.

Topics will include the large-scale circulation, boundary and interior mixing, cross-equatorial transports and processes, ventilation and water mass formation, heat and freshwater transport and surface fluxes and the connection with the Southern Ocean. Special sessions will be devoted to results from the Deep Basin Experiment in the Brazil Basin. Particular emphasis will be given to data-model comparisons and the related numerical and inverse modelling and assimilation.

The workshop will consist in a mix of overview papers, shorter contributed papers, poster and computer presentations, and working group sessions centred on specific scientific or scientific/technical issues.

As with companion WOCE workshops, it is expected that a proceedings, or a special issue of an appropriate journal, will be published after the meeting, but its scope, content and timetable will be decided nearer the workshop date.

Planning and organization of the workshop will be greatly facilitated if initial interest in participation is indicated before 31 October 1996. Such indication should include specific area of interest, and be directed to:

Yves Desaubies
Laboratoire de Physique des Océans
Unité Mixte de Recherche
CNRS - IFREMER - UBO IFREMER
BP 70 29280 Plouzané
France
Tel: (33) 98 22 42 75
FAX: (33) 98 22 44 96
e-mail: yves.desaubies@ifremer.fr

Scientific Organizing Committee:

B. Barnier
Y. Desaubies (Chair)
S.L. Garzoli
N. Hogg
J.R. Lutjeharms
H. Mercier
W. Roether
P. Saunders
G. Siedler.

The Latest International WOCE Publications

131/95 WOCE INTERNATIONAL PROJECT OFFICE. 1995. The WOCE Handbook, 6th edition: A guide to WOCE scientific infrastructure for 1995. 35pp.

132/95 WOCE INTERNATIONAL PROJECT OFFICE. 1995. Report of the eighth meeting of the WOCE Data Products Committee (DPC-8), Florida State University Center for Professional Development, Tallahassee, FL, USA, 24–27 April 1995. 26pp.

133/95 WOCE INTERNATIONAL PROJECT OFFICE. 1995. Workshop for Quality Control of WOCE Upper Ocean Thermal Data, Scripps Institution of Oceanography, 22–25 May 1995. 18pp.

134/95 IOC/WMO. WOCE Surface Velocity Programme Barometer Drifter Construction Manual. 1995. Sybrandy, A.L., C. Martin, P. Niiler, E. Charpentier and D.T. Meldrum. (Data Buoy Cooperation Panel). DBCP Technical Document No. 4. 63pp.

135/95 WOCE DATA INFORMATION UNIT. 1995. WOCE Data Handbook (3rd edition). Looseleaf.

136/96 WOCE INTERNATIONAL PROJECT OFFICE. 1996. Report of the Fourteenth Meeting of the WOCE Hydrographic Programme Planning Committee (WHP-14), Bundesamt für Seeschiffahrt und Hydrographie, Hamburg, Germany, 10–12 October 1995. 31pp.

137/96 IOC/UNESCO. 1996. Third Session of the IOC-WMO Intergovenmental WOCE Panel (IWP-3), Paris, 8–9 June 1995. 122pp.

138/96 WOCE INTERNATIONAL PROJECT OFFICE. 1996. WOCE Project Status 1996: Future Aims. 8pp.

139/96 WOCE INTERNATIONAL PROJECT OFFICE. 1996. Report of the Fourth Meeting of the CLIVAR-WOCE XBT/XCTD Programme Planning Committee (CWXXPPC-4), Marine Environmental Data Service, Ottawa, Canada, 12–13 October 1995. 42pp.

140/96 WOCE INTERNATIONAL PROJECT OFFICE. Report of the Twenty-Second Meeting of the WOCE Scientific Steering Group (WOCE-22), Woods Hole Oceanographic Institution, Woods Hole, MA, USA, 30 October – 1 November 1995. 35pp.

141/96 COAPS. 1996. Handbook of Quality Control Procedures and Methods for Surface Meteorology Data. Smith, S.R., C. Harvey and D.M. Legler. COAPS Technical Report No. 96-1. 52pp.

142/96 WOCE INTERNATIONAL PROJECT OFFICE. 1996. Report of the Ninth Meeting of the WOCE Data Products Committee (DPC-9), IFREMER, Brest, France, 6–9 February 1996. 22pp.

143/96 WOCE HYDROGRAPHIC PROGRAMME SPECIAL ANALYSIS CENTRE. 1996. A New Hydrographic Dataset for the South Pacific: Synthesis of WOCE and historical data. Gouretski, V., and K. Jancke.

Note on Copyright

WOCE is a component of the World Climate Research Programme (WCRP), which was established by WMO and ICSU, and is carried out in association with IOC and SCOR. The scientific planning and development of WOCE is under the guidance of the Scientific Steering Group for WOCE, assisted by the WOCE International Project Office.

The WOCE Newsletter is edited at the WOCE IPO at the Southampton Oceanography Centre, Empress Dock, Southampton SO14 3ZH (Tel: 44-1703-596789, Fax: 44-1703-596204, e-mail: woceipo@soc.soton.ac.uk).

We hope that colleagues will see this Newsletter as a means of reporting work in progress related to the Goals of WOCE as described in the Scientific Plan. The SSG will use it also to report progress of working groups, experiment design and models.

The editor will be pleased to send copies of the Newsletter to institutes and research scientists with an interest in WOCE or related research.

Printed by the Design and Print Centre of the University of Southampton